Cold-induced expression of a truncated Adenylyl Cyclase 3 acts as rheostat to brown fat function.

Sajjad Khani[1,2$], Hande Topel[3$], Ajeetha Josephrajan[3], Bjørk Ditlev Marcher Larsen[3], Ana Rita Albuquerque de Almeida Tavanez[3], Michael James Gaudry[4], Philipp Leyendecker[5], Natasa Stanic[3], Isabella Gaziano[2], Nils Rouven Hansmeier[2], Elena Schmidt[2], Paul Klemm[2], Lara-Marie Vagliano[5], Christoph Andreas Engelhard[3,6], Søren Nielsen[6], Naja Zenius Jespersen[6], Rizwan Rehimi[7] , Sabrina Gohlke[8], Peter Frommolt[9], Thorsten Gnad[10], Alvaro Rada-Iglesias[11], Marta Pradas-Juni[12], Tim Julius Schulz[8], Frank Thomas Wunderlich[2], Alexander Pfeifer[10], Martin Jastroch[4], Dagmar Wachten[5#] and Jan-Wilhelm Kornfeld[2,3#]

Affiliations:

[1]Institute for Genetics, University of Cologne, Zülpicher Str. 47aD-50674 Cologne, Germany. [2]Max-Planck Institute for Metabolism Research, Gleueler Strasse 50, 50931 Cologne, Germany. [3]Department for Biochemistry and Molecular Biology, University of Southern Denmark, Campusvej 55, 5230 Odense, Denmark. [4]Department of Molecular Biosciences, The Wenner-Gren Institute, Stockholm University, SE-106 91, Stockholm, Sweden. [5]Institute of Innate Immunity, Medical Faculty, University of Bonn, Venusberg-Campus 1, 53127 Bonn, Germany. [6]Centre for Physical Activity Research, Department of Infectious Diseases, Rigshospitalet, Faculty of Health Sciences, University of Copenhagen, Blegdamsvej 9, 2100 Copenhagen, Denmark. [7]Center for Molecular Medicine Cologne (CMMC), University of Cologne, Robert-Koch-Str. 2150931 Cologne, Germany. [8]Department of Adipocyte Development and Nutrition, German Institute of Human Nutrition Potsdam-Rehbrücke, Arthur-Scheunert-Allee 114-116, 14558 Nuthetal, Germany. [9]Institute of Human Genetics, University Medical Center Hamburg-Eppendorf, Martinistr. 52, 20246 Hamburg, Germany. [10]Institute of Pharmacology and Toxicology, University Hospital, University of Bonn, Venusberg-Campus 1, 43127, Bonn, Germany. [11]Institute of Biomedicine and Biotechnology of Cantabria (IBBTEC), CSIC/University of Cantabria, C/ Albert Einstein 22, 39011 Santander. [12]Novo Nordisk Foundation Center for Basic Metabolic Research (CBMR), Blegdamsvej 3a, 2200 Copenhagen, Denmark.

[$,#] = These authors contributed equally to this work.

Abstract:

Promoting brown adipose tissue (BAT) activity has been recognized as innovative therapeutic approach to improve obesity and metabolic disease. Whilst the molecular circuitry underlying thermogenic activation of BAT is well understood, the processes underlying rheostatic regulation of BAT to maintain homeostasis and avoid excessive energy dissipation remain ill-defined.

Increasing cyclic AMP (cAMP) biosynthesis is key for BAT activation. Here, we demonstrate that ADCY3, an adenylyl cyclase whose expression is induced during cold exposure and regulates cAMP homeostasis in thermogenic fat, is dispensable for BAT function in lean mice, but becomes critical during obesity. Furthermore, by combining RNA-seq with epigenomic H3K4me3 profiling, we detected a novel, cold-inducible promoter that generates a 5' truncated *Adcy3-at* mRNA isoform, *Adcy3-at*. Mice lacking only *Adcy3-at*, but not *full-length Adcy3*, displayed increased energy expenditure already under lean conditions and were protected against obesity and ensuing metabolic imbalances. Subcellularly, translated ADCY3-AT proteins are retained in the endoplasmic reticulum (ER), did not translocate to the cell membrane, and lacked enzymatic activity. By interacting with ADCY3, ADCY3-AT retained ADCY3 in the ER and, thereby, reduced the plasma membrane pool of ADCYs available for G-protein mediated cAMP synthesis. Thereby, ADCY3-AT acts as a signaling rheostat in BAT, limiting adverse consequences of uncurbed cAMP activity after long-term BAT activation. *Adcy3-at* induction was driven by a cold-induced, truncated isoform of the transcriptional cofactor PPARGC1A (PPARG Coactivator 1 Alpha, PPARGC1A-AT). Expression of *Ppargc1a-at* and *Adcy3-at* are evolutionary conserved, indicating that transcriptional rewiring by commissioning of alternative promoters is key for thermogenic fat function.

53 ***Introduction:***

54 Most mammals harbor two morphologically and functionally distinct types of adipocytes (fat cells):
55 White adipocytes consist of a single lipid droplet[1] and predominantly regulate energy storage,
56 whereas brown adipocytes are multilocular and possess the ability to convert (diet-derived)
57 macronutrients like carbohydrates and lipids into heat in a unique molecular process termed Non-
58 Shivering Thermogenesis (NST)[2]. Interest in brown adipose tissue (BAT) arose after the seminal
59 discovery that *(i)* BAT not only exists in small animals like rodents and in human infants, but that
60 adult humans can possess active brown fat [3-5] and *(ii)* cold ambient temperature exposure or
61 stimulation of beta-adrenergic G-Protein receptors (GPCRs) activates BAT, which positively
62 correlates with energy expenditure[6] and inversely correlates with body-mass indices[7, 8].

63 GPCRs regulate a plethora of biological processes and are the target of a major part of drugs in
64 clinical use[9]. GPCRs play a central role in adipose tissue homeostasis, and adipocyte metabolism
65 is regulated by GPCRs linked to different functional classes of heterotrimeric G proteins [10]. The
66 main physiological stimulus for NST in brown and thermogenically activated 'brite' (brown-in-
67 white) fat is cold temperature, which activates the sympathetic nervous system (SNS) and leads to
68 release of the neurotransmitter norepinephrine (NE) [11]. NE activates beta-adrenergic GPCRs[12],
69 which then stimulate synthesis of the second-messenger 3'-5'-cyclic adenosine monophosphate
70 (cAMP) by plasma membrane-bound adenylyl cyclases[13, 14] and activates protein kinase A (PKA),
71 thereby inducing lipolysis. The ensuing generation of free fatty acids (FFA) activates uncoupling
72 protein 1 (UCP1), a mitochondrial protein whose activation executes NST in brown and brite fat[2].
73 In addition to these acute effects, chronic cAMP signaling is required for adipocyte precursor
74 differentiation [2]. Adenylyl cyclase 3 (ADCY3), which is expressed in somatic tissues like adipose
75 tissue, kidney, pancreas and liver as well as in olfactory sensory and hypothalamic neurons[15],
76 received attention due to loss-of-function variants in human *ADCY3* that correlate with enhanced
77 susceptibility to increased BMI[16] and *ADCY3* loss-of-function mutations cause severe obesity in
78 multiple human populations [17-19]. Mouse studies confirmed that *Adcy3* silencing is sufficient to
79 impair energy homeostasis [20-24], yet the precise role of ADCY3 in thermogenic fat has not been
80 addressed yet.

81 Pre-mRNA splicing is a fundamental gene-regulatory mechanism that enables cells to increase
82 proteome complexity from a finite amount of exonic information and is important for adipocyte
83 function, cold tolerance, and metabolic health [25-27] . For instance, PPARG coactivator 1 alpha
84 (PPARGC1A), a key transcriptional regulator in adipose tissue, displays an alternative 5' promoter
85 in human muscle, generating a C-terminally truncated protein that elicits distinct transcriptional
86 programs [28, 29]. It remains elusive though if similar alternative promoter events contribute to
87 metabolic regulation in thermogenic fat. *Here, we describe a novel molecular rheostat, ADCY3-*

88 *AT, that is selectively induced and controls brown fat function upon cold and beta-adrenergic*
89 *stimulation. N-terminally truncated ADYC3-AT proteins limit cAMP synthesis by controlling the*
90 *subcellular localization of adenylyl cyclases and ultimately energy dissipation. Truncated ADCY3*
91 *is evolutionary conserved in brown adipocytes from rodents to humans and is part of a conserved*
92 *transcriptional network, linking thermogenic activation to adaptive proteoform changes.*
93
94 ***Results:***
95 ***Transcriptional regulation of cAMP biosynthesis during cold adaptation of brown adipose tissue.***
96 To identify transcriptional processes controlling 3',5'-cyclic adenosine monophosphate (cAMP)
97 second messenger production in cold-activated brown (BAT) and epididymal white adipose tissue
98 (eWAT), we exposed chow diet-fed, male C57BL/6N mice to 24 hours of 5°C cold exposure (CE)
99 and analyzed transcriptome-wide gene expression changes using mRNA-sequencing (RNA-seq).
100 We combined our analysis with public mRNA-seq data from 72 h cold-exposed, inguinal white
101 adipose tissue (iWAT)[30] and observed significantly (FDR ≤ 0.05) up-or downregulated genes,
102 respectively: 1,086/1,204 genes in BAT, 804/448 genes in iWAT, and 584/71 in eWAT (Fig.1a-c,
103 Fig.S1a-c) genes between cold and ambient room (22°C) temperatures (s. Supplemental table S1).
104 KEGG gene ontology (GO) analysis revealed that peroxisome and PPAR signaling, as well as
105 protein metabolism processes were induced, whereas HIF-1-dependent hypoxic signaling was
106 repressed in cold-activated BAT (Fig.1d). Canonical thermogenic and brown-fat associated GO
107 terms like oxidative phosphorylation, thermogenesis, tricarbon acid cycle, and carbon metabolism
108 were upregulated in iWAT (Fig.1e), whereas few categories were altered in eWAT (Fig.1f), likely
109 reflecting the limited capacity for thermogenesis in this depot. We next specifically investigated
110 the expression of cAMP-degrading and synthesizing enzymes: Whilst expression of negative
111 regulators of cyclic nucleotides, namely 3′,5′-cyclic nucleotide phosphodiesterases (PDEs)[31],
112 remained unchanged across all depots investigated (Fig.S1d-f), mRNA levels of adenylyl cyclase
113 isoforms 3 and 4 (*Adcy3*, *Adcy4*) were specifically induced in cold-exposed BAT (Fig.1g) and only
114 *Adcy3* expression was induced in iWAT (Fig.1h), whereas expression of *Adcy* isoforms remained
115 unaltered in eWAT (Fig.1i). These results point towards a specific role for ADCY3 in thermogenic
116 adipocytes and regulation of energy expenditure as proposed previously [32, 33].
117 Analysis of public single-nuclei RNA-Seq (snRNA-seq) datasets[34] from purified brown adipocytes
118 (BA) revealed that *Adcy3* is expressed lowly under basal (thermoneutral) conditions not exhibiting
119 substantial NST. However, *Adcy3* expression is induced when lowering ambient temperatures from
120 thermoneutrality (TN) to room temperature (RT) to cold exposure (CE) in brown adipocytes (BAs),
121 paralleling increased expression changes of known BAT markers like uncoupling protein 1 (*Ucp1*,
122 Fig.1j). Similar patterns were observed for known BAT markers[35] like PPARGC1A, pyruvate

123 dehydrogenase kinase 4 *(Pdk4)*, PR/SET domain 16 *(Prdm16),* and cell death inducing DFFA like
124 effector A *(Cidea*, Fig.1k). Thus, cold activation induces *Adcy3* expression in cold-activated BA
125 and inguinal white adipocytes (iWA).
126
127 ***ADCY3 is required for cAMP biosynthesis in BAT and required for cold adaptation in obesity.***
128 To decipher the adipocyte-autonomous roles of ADCY3 *in vivo*, we next crossed mice harboring
129 *LoxP*-flanked *Adcy3* alleles[24] with animals expressing Adiponectin (*Adipoq*)-promoter driven cre
130 recombinase[36] (*Adipoq-cre*) to obtain pan-adipocyte-deficient *Adcy3* knockout mice (*Adcy3*$^{LoxP/LoxP}$,
131 *Adipoq-cre*$^{+/cre}$; *Adcy3-AdcKO)* and cre-negative littermates *(Adcy3*$^{LoxP/LoxP}$*, Adipoq-cre*$^{+/+}$; *LoxP*,
132 Fig.2a*)*. RNA-seq demonstrated 60-70% reduction of *Adcy3* in *Adcy3-AdcKO* BAT with remaining
133 *Adcy3* likely representing non-adipocyte cell populations in BAT[34] (Fig.2b). Cyclic AMP levels in
134 BAT of mice housed at room temperature were concomitantly reduced 50 %, pointing to ADCY3
135 constituting a pivotal cAMP regulator in thermogenic fat (Fig.2c). To probe for roles of adipocyte
136 ADCY3 in energy metabolism, we analyzed metabolic parameters in lean, chow diet-fed *Adcy3-*
137 *AdcKO* mice. Unexpectedly, we observed no differences in body weight (BW, Fig.2d), and
138 intraperitoneal glucose (Fig.2e) and insulin (Fig.2f) tolerance tests revealed no differences in
139 glucose metabolism between chow diet-fed, lean *Adcy3-AdcKO* and *LoxP* control mice. We also
140 performed indirect calorimetry assessment of energy homeostasis at 22°C and 5°C but found no
141 differences in respiratory exchange ratios (RER, Fig.2g).
142 In line with little overt metabolic effects following *Adcy3* loss *in vivo*, we detected no differences
143 in regulation of genes involved in thermogenic activation in *Adcy3-AdcKO* BAT at 22°C and 5°C
144 (Fig.S3a,b). We also investigated thermogenic activation in mature *Adcy3*-deficient BAs *in vitro*
145 and committed *(i) Adcy3-AdcKO* stromal-vascular fraction-derived progenitor cells (SVF) or *(ii)*
146 *LoxP* SVFs in mature BA, transduced *LoxP*-derived BAs with adeno-associated virus 8 (AAV8)
147 encoding Cre (AAV8-cre), followed by CL316,243 stimulation of both models, genetic and viral.
148 *Adcy3*-deficient and control cells showed neither changes in adipocyte identity markers like *Pparg2*
149 and *Fabp4* nor in activation upon beta-adrenergic treatment, despite *Adcy3* silencing in both
150 (Fig.S2c-d), suggesting unaltered BA formation and activation. Of note, we saw progressive trends
151 towards impaired oxygen consumption (Fig.2h-i) and locomotor activity (Fig.2j), suggesting mildly
152 impaired cold tolerance during prolonged cold exposure in *Adcy3-AdcKO* mice. Thus, adipocyte-
153 specific loss of *Adcy3* only marginally affects thermogenesis and metabolic function in lean mice,
154 but despite controlling cAMP levels in BAT, does not represent a major regulator for cAMP-
155 dependent thermogenesis.
156

157 We and others reported that impediment of BAT function predisposes mice to increased body
158 weight gain and metabolic deterioration when feeding obesogenic high-fat diets (HFD) [37-41]. Given
159 the modest effects of ADCY3 deficiency on energy expenditure in lean mice, we next asked if HFD
160 renders *Adcy3-AdcKO* mice more susceptible to metabolic complications. We again observed no
161 genotype-specific differences in BW (Fig.2k), adipose tissue weights (Fig.S3a-b), glucose (Fig.2l)
162 or insulin tolerance (Fig.2m). When performing indirect calorimetry, obese *Adcy3-AdcKO* mice
163 displayed a reduction in RER (Fig.2n) compared to lean mice (Fig.2g), reflecting a transition in
164 substrate mobilization from carbohydrate to lipid oxidation in diet-induced obesity (DIO), yet no
165 Adcy3-driven differences were seen. In contrast, oxygen consumption (Fig.2o) and activity
166 (Fig.2p) were reduced in obese *Adcy3-AdcKO* mice compared to HFD-fed *LoxP* controls. Thus,
167 fat-specific loss of *Adcy3* in mice reduces energy expenditure in obese mice, also during cold stress.
168
169 ***ADCY3 loss causes precocious activation of PKA-independent signaling pathways***
170 Intrigued by the lack of thermogenic and metabolic dysfunction in lean *Adcy3-AdcKO* mice, we
171 tested whether *Adcy3* loss in adipocytes rewired cAMP signaling. To test whether kinase activities
172 are altered in *Adcy3-AdcKO* BAT, we first performed Western Blot activity profiling using PKA
173 substrate-specific phospho-antibodies and analyzed UCP1 protein expression. In line with lack of
174 thermogenic dysfunction in lean mice, PKA substrate activation and UCP1 protein levels in BAT
175 after chronic cold exposure were upregulated to same degrees in *LoxP* and *Adcy3-AdcKO* mice
176 (Fig.S3c). To test more broadly the effects of *Adcy3* deficiency on signaling responses, we carried
177 out serine/threonine kinase (STK) profiling using PamGene peptide arrays to globally infer
178 differential STK kinase activities in *Adcy3-AdcKO* BAT. In *LoxP* mice, acute cold exposure (24 h)
179 elicited only mild overall STK signaling responses (Fig.S3d), whereas chronic cold stimulation for
180 6 days decreased the activity of members of the CMGC kinase family (including cyclin-dependent
181 kinases (CDK), glycogen synthase kinases (GSK) and MAP kinases (MAPK)), and activity of AGC
182 family members (including protein kinase A (PKA), C (PKC), and G (PKG) were elevated
183 (Fig.S3ei,ii). The CMGC family includes important hubs of cAMP-dependent signaling like the
184 MAPKs p38 [42], ERK [43], JNK [44], which are typically engaged during acute thermogenic activation[45].
185 However, STK signatures in BAT of *Adcy3-AdcKO* at 22°C resembled chronic cold exposure in
186 *LoxP* mice with exception that PKA activity remained unchanged (Fig.S3f, i-iii). Thus, kinase
187 signaling pathways regulating BAT activation are indeed rewired in *Adcy3-AdcKO* mice but
188 independent of PKA signaling. This is reflected on the functional level as minor metabolic changes
189 were observed in lean *Adcy3-AdcKO* mice at room temperature. Only when coupled to an additional
190 obesity burden, *Adcy3-AdcKO* are sensitive to metabolic deterioration.
191

192 ***Active thermogenic adipocytes express a truncated ADCY3 (ADCY3-AT) transcript and protein***
193 ***isoform***
194 Chromatin profiling by chromatin-immunoprecipitation-sequencing (ChIP-seq) allows genome-
195 wide mapping of DNA-regulatory elements and changes in cellular energetic activation and/or
196 differentiation are paralleled by profound remodeling of promoter (e.g., H3K4me3) and enhancer
197 (e.g., H3K27Ac)-associated histone post-translational modifications in BA[46-48]. When interrogating
198 previously published H3K4me3 data from BAT of cold-exposed mice[49], we observed a H3K4me3-
199 marked promoter in intron 2 of the *Adcy3* gene that arose during cold (Fig.S4a), which we verified
200 by ChIP-qPCR (Fig.S4b). This promoter marked a cold-dependent novel transcriptional start site
201 giving rise to a 5'-truncated *Adcy3* mRNA isoform (Fig.S4a), which we termed *Adcy3-at* to discern
202 it from GENCODE annotated full-length *Adcy3* (*Adcy3-fl*). When combining Illumina short-read
203 with Oxford Nanopore Technology full-length RNA-seq from cold-activated BAT, we confirmed
204 that *Adcy3-at* represents a contiguous transcript ranging from *Adcy3-at* TSS in exon 2b to exon 22
205 (Fig.3a). *Adcy3-at* encoded ADCY3-AT proteins are predicted as N-terminally truncated compared
206 to full-length ADCY-FL proteins (Fig.3b) and distinct from ADCY3 loss-of-function protein
207 isoforms previously reported in human populations [17-19]. Thus, cold exposure activates an intronic
208 *Adcy3* promoter that produces N-terminally truncated, unannotated *Adcy3-at* mRNA isoform in
209 thermogenic fat depots.
210
211 When analyzing our RNA-seq data separately for *Adcy3-at* and *Adcy3-fl* isoform expression, we
212 found that predominantly *Adcy3-at* was induced during cold exposure and constituted the dominant
213 *Adcy3* isoform after cold as shown by RNA-seq (Fig.3c-d) and qPCR (Fig.3e) quantification. Other
214 thermogenic depots like iWAT also induced *Adcy3-at* in cold (Fig.3f), whilst eWAT *Adcy3-at*
215 induction was not significant (Fig.3g), pointing to roles of ADCY3-AT in thermogenic processes
216 in mature BA, yet effects of ADCY3-AT on brown adipogenesis were not addressed at point. To
217 address this important point specifically, we analyzed *Adcy3* isoform expression during adipogenic
218 differentiation and observed that *Adcy3-at* expression was low throughout adipogenesis of BAT
219 SVFs into BA and was only upregulated upon dibutyryl (db)-cAMP and CL316,243 stimulation
220 (Fig.S4e), whereas *Ucp1* and *Adcy3-fl* expression was more highly expressed during brown
221 adipogenesis (Fig.S4f-g). *Adcy3-at* was upregulated in a cell-autonomous manner in primary brown
222 adipocytes (1°BA) and primary inguinal white adipocytes (1°iWA), yet only trended towards
223 induction in primary epididymal white adipocytes (1°eWA) after stimulation with beta3-adrenergic
224 agonist CL316,243 in all depots (Fig.3h-j). *Adcy3-fl*, but especially *Adcy3-at*, were expressed at
225 low abundance in non-adipose metabolic tissues like liver, skeletal muscle, kidney, and pancreas
226 (Fig.S4c-d). In obesity- and aging-associated adipose dysfunction, *Adcy3-at* expression was

227 unchanged in BAT and downregulated in iWAT of DIO mice, a finding seen for canonical BAT
228 markers like *Ucp1*, Iodothyronine Deiodinase 2 (*Dio2*) and ELOVL fatty acid elongase 3 (*Elovl3*,
229 Fig.S4h,i). *Adcy3-at* expression was also unaffected in BAT of aged (25 months-old) compared to
230 young (2 months-old) C57BL/6N male mice (Fig.S4j). Thus, two mouse models of functional
231 thermogenic decline [50] showed no differences in BAT *Adcy3-at* expression.
232 The ADCY3-AT and ADCY3-FL amino acid (aa) sequences are for large parts identical but differ
233 at the N-terminus: ADCY3-AT lacks 146aa and instead contains a novel 28aa N-terminus, entailing
234 that ADCY3-AT proteins specifically lack the 1st block of transmembrane (TM) domains, which
235 constitutes an integral structural hallmark and functional feature of most adenylyl cyclases (Fig.3b).
236 When performing Western blot analysis using a C-terminal pan-ADCY3 antibody, we detected an
237 additional ADCY3-specific signal at ca. 70 kD after 24 h of db-cAMP and CL316,243 stimulation
238 in 1°BA and 1°WA, which was absent in unstimulated cells (Fig.3k-l), likely representing ADCY3-
239 AT proteins. Thus, pharmacological and cold temperature-mediated activation of thermogenic
240 adipocytes leads to presence of a novel intronic *Adcy3-at* promoter that encodes truncated ADCY3-
241 AT proteins.
242
243 ***ADCY3-AT inhibits oxidative metabolism in vitro and in vivo.***
244 As *Adcy3-AdcKO* mutants were deficient for both *Adcy3* isoforms (Fig.3c-d), we tested the specific
245 role of ADCY3-AT in cellular and metabolic homeostasis of BA *in vivo* and *in vitro.* We performed
246 CRISPR-Cas9-mediated gene deletion using single-guide RNAs (sgRNAs) flanking the H3K4me3-
247 marked *Adcy3-at* promoter and excised a 978 bp-long DNA fragment including the *Adcy3-at* TSS
248 in embryonic stem cells (Fig.S5a). Excision of *Adcy3-at* TSS and promoter regions was confirmed
249 by Southern blot (Fig.S5b) and genomic PCR analysis (Fig.S5c). Homozygous ADCY3-AT null
250 animals, henceforth termed *Adcy3ΔAT*, exhibited no overt phenotypes, were fertile in both sexes,
251 and *Adcy3ΔAT* alleles were inherited at Mendelian ratios, arguing against confounding
252 developmental defects after *Adcy3-at* deletion. Importantly, *Adcy3ΔAT* mice were devoid of *Adcy3-*
253 *at* (Fig.4b), but not *Adcy3-fl* (Fig.4c).
254
255 First, we tested the role of ADCY3-AT in regulating energy homeostasis in lean mice: Although
256 BW remained unchanged (Fig.4d), *Adcy3ΔAT* animals exhibited improved glucose tolerance
257 (Fig.4e) despite even mildly increased food intake (Fig.4f), normal insulin sensitivity (Fig.S5d) and
258 unaltered locomotor activity (Fig.S5e), suggesting negative energy balance in *ADCY3ΔAT* mice.
259 RER quotients unveiled that *Adcy3ΔAT* animals trended towards increased carbohydrate usage at
260 22°C (Fig.S5f), likely reflecting an increased capacity of *ADCY3ΔAT* mice for enhanced glucose
261 disposal, which consequently exhibited trends towards increased oxygen consumption during 22°C

262 and 5°C ambient temperatures (Fig.4g). To test for BAT-specific involvement in the improved
263 metabolism seen in *Adcy3ΔAT* mice, we performed qPCR analysis and observed trends towards
264 increased *Ppargc1a* and *Prdm16* expression, suggesting mildly elevated activation of cold-
265 acclimatized *Adcy3ΔAT* BAT (Fig.4h). Notably, expression of gene markers reflecting myogenic-
266 to-BA remodeling, such as myosin heavy chain 1 *(Myh1)* and 4 (*Myh4*), ryanodine receptor 1
267 *(Ryr1)*, ATPase sarcoplasmic/endoplasmic reticulum Ca2+ transporting 1 *(Atp2a1)*, troponin T3
268 fast skeletal type *(Tnnt3)*, actin alpha 1, skeletal muscle *(Acta1)*, troponin I2, fast skeletal type
269 *(Tnni2)*, H19 imprinted maternally expressed transcript *(H19)*, creatine kinase, M-type *(Ckm)*,
270 tropomyosin 1 and 2 (*Tpm1,2*) were repressed (Fig.4i), reflecting transcriptional signatures
271 reminiscent of activated BA at the expense of myogenic gene expression in *Adcy3ΔAT* mice, a
272 change in transcriptional signatures reported for other models of BAT gain-of-function [38, 40].
273
274 Albeit these mild increases in energy dissipation, we hypothesized that *Adcy3ΔAT* mice are
275 protected against DIO-induced metabolic alterations. To test this, we exposed *LoxP* and *Adcy3ΔAT*
276 to HFD feeding and observed that *Adcy3ΔAT* were indeed protected against DIO-associated BW
277 gains and glucose intolerance (Fig.4j-k) and *Adcy3ΔAT* mice exhibited lower glucose levels during
278 an insulin challenge (Fig.S5h). As seen in chow diet-fed animals, obese *Adcy3ΔAT* exhibited
279 decreased myogenic gene expression reflecting increased BA activation (Fig.4l). To test for BA-
280 intrinsic roles of ADCY3-AT, we performed Seahorse bioenergetic analyses in 1°BA and 1°iWA
281 and observed elevated maximal oxygen consumption rates after CL316,243 stimulation (Fig.4m)
282 and during FCCP treatment in mitochondrial stress tests in *Adcy3-at* deficient adipocytes (Fig.4o).
283 Together with higher extracellular acidification rates in *Adcy3ΔAT* cells (Fig.4n,p), the results
284 indicated a combination of increased oxidative phosphorylation and glucose oxidation in
285 *Adcy3ΔAT* 1°BA (Fig.4m-p) and 1°WA (Fig.S5i-l). Thus, ADCY3-AT deficiency improves
286 metabolism *in vivo*, especially upon diet-induced obesity, by increasing energy dissipation in brown
287 adipocytes and myogenic-to-BA transcriptional remodeling.
288
289 ***ADCY3-AT alters ADCY3-FL subcellular localization and thereby limits cAMP biosynthesis.***
290 Our *in vitro* and *in vivo* data thus far indicated that silencing of cold-inducible ADCY3-AT
291 increases oxidative metabolism and thermogenic activation of BA. To test this molecularly, we
292 analyzed STK activities using PamGene Array analysis in BAT of *Adcy3ΔAT*. At 22°C, STK
293 activity in *Adcy3ΔAT* BAT remained largely unchanged compared to BAT from *LoxP* control mice
294 (Fig.S6a), demonstrating that ADCY3-AT does not profoundly affect STK kinase activity under
295 basal conditions. Upon chronic cold stimulation, directional changes in kinase activities in
296 *Adcy3ΔAT* were comparable also to cold-exposed *LoxP* mice (Fig.S6b). Importantly, when

297 comparing kinase activity in BAT from *Adcy3ΔAT* with *Adcy3-AdcKO*, signaling inversely
298 correlated, indicating that deleting both ADCY3 proteins evokes opposing effects to ablating
299 ADCY3-AT alone (Fig.S6c-d).
300
301 The presence of ADCY3-AT coincides with ADCY3-FL in activated BAT (Fig.3b,c), yet the
302 functional implication of this co-expression remained elusive. Adenylyl cyclases are active as
303 protein dimers, and dimerization affects protein transport to the plasma membrane (PM). Besides
304 homodimerization, ADCYs can also assemble in heterodimers between different adenylyl cyclase
305 isoforms[51]. We thus hypothesized that ADCY3-AT controls the activity of ADCY3-FL by protein
306 interaction. To test this notion *in vitro*, we co-expressed FLAG-tagged ADCY3-AT and HA-tagged
307 ADCY3-FL in Chinese Hamster Ovary (CHO) cells and demonstrated by co-immunoprecipitation
308 that ADCY3-AT and ADCY3-FL indeed interact (Fig.5a-b). The N terminus of adenylyl cyclases
309 control transport to PM, thereby regulating its localization and, concomitantly, enzymatic function
310 [52]. As ADCY3-AT lacks the N-terminal domain and interacts with ADCY3-FL, we next tested if
311 ADCY3-AT might not be able to localize to the PM, and in turn, also impairs membrane transport
312 of ADCY3-FL. To this end, we performed biotinylation assays to selectively labeled TM proteins
313 that face the extracellular *environment*. When individually overexpressing the two different
314 isoforms, only ADCY3-FL, but not ADCY3-AT, was biotinylated (Fig.5c-d), demonstrating that
315 ADCY3-AT does not localize to the PM. To complement this result with image-based approaches,
316 we subjected CHO cells grown on glass coverslips to short ultrasound pulses, whereby the upper
317 part of cells was removed and the PM and its associated complexes remained intact as membrane
318 sheets ('unroofing')[53]. As positive control for visualizing the PM, we expressed membrane-
319 anchored mCherry. ADCY3-FL colocalized with mCherry in the PM, but showed little overlap
320 with calnexin, a protein residing in the ER membrane and here specifically marking ER-PM contact
321 sites. In contrast, ADCY3-AT showed no colocalization with mCherry, but colocalized with
322 calnexin, demonstrating that ADCY3-AT is retained in the ER (Fig.5e-f, Fig.S6e-f). Upon co-
323 expression of ADCY3-AT and ADCY3-FL, ADCY3-FL was retained in the ER and no longer
324 localized to the PM, indicating that interaction of ADCY3-AT with ADCY3-FL prevented PM
325 trafficking of ADCY3-FL proteins (Fig.5g, Fig.S6g). To probe if ADCY3-AT intrinsically
326 possesses cAMP catalytic activity, we determined cAMP levels by ELISA in CHO cells
327 overexpressing the individual ADCY3 isoforms. As expected, ADCY3-FL, but not ADCY3-AT,
328 activity was stimulated with forskolin, a direct ADCY activator (Fig.S6h), and isoproterenol, a
329 beta-adrenergic receptor agonist, which stimulates adenylyl cyclase activity via G-proteins
330 (Fig.S6i), indicating that ADCY3-AT does not possess enzymatic activity or lost its interaction
331 with G-proteins due to altered subcellular localization. Our hypothesis that ADCY3-AT/ADCY3-

332 FL heterodimer formation is favored in cold-activated BAT was supported by *in silico* modeling of
333 ADCY3-AT and ADCY3-FL heteromeric structures using AlphaFold [54]. Our structural modelling
334 suggested that ADCY3 heterodimer are energetically plausible (Fig.5h), underlining that ADCY3-
335 AT-mediated retention of ADCY3-FL represents a credible scenario for ADCY3-AT-mediated
336 repression of adenylyl cyclase activity. Thus, in the presence of both isoforms, ADCY3-AT and
337 ADCY3-FL, ADCY3-FL transport to PM in ADCY3-AT/FL heterodimrs is impaired, suggesting
338 that interaction of ADCY3-AT with ADCY3-FL curbs cytoplasmic cAMP production by altered
339 localization and/or cAMP compartmentalization.
340
341 ***Conserved and cold-inducible PPARGC1A -AT drives Adcy3-at expression in brown adipocytes.***
342 PPARGC1A represents a central regulator of mitochondrial biogenesis [29, 55] and is imperative for
343 brown adipocyte differentiation and function [56]. Intriguingly, alternative splicing-mediated removal
344 of exons 6-7 of *Ppargc1a* has been reported to results in C-terminally truncated NT-PGC1alpha [57-
345 59]. Loss of NT-PGC1alpha protects against obesity [60], suggesting negative roles for truncated
346 PPARGC1A protein isoforms in BA differentiation and/or function. Beyond NT-PGC1alpha,
347 alternative promoter usage and alternative splicing events give rise to more than ten PPARGC1A
348 proteoforms, each coordinating tissue- and state-dependent adaptive transcriptional processes [29, 61].
349 When interrogating our Illumina and Nanopore RNA-seq data, we observed the cold-induced
350 alternative promoter accrual and generation of a novel transcript start site 5' of the canonical, full-
351 length *Ppargc1a* (*Ppargc1a-fl*, i.e. the *Pgc1alpha1* isoforms reported previously[61]) TSS, giving rise
352 to a novel *Ppargc1a* mRNA isoform. In analogy to *Adcy3-at* we termed this 5'-terminally truncated
353 mRNA isoform *Ppargc1a-at* (Fig.6a). *Ppargc1a-at* encoded a C-terminally truncated PPARGC1A-
354 AT proteoform (Fig.6b) that represents a murine homologue to the *Ppargc1alpha4* isoform
355 reported for human skeletal muscle [28]. As PPARGC1A, together with cognate nuclear hormone
356 transcription factors, controls adaptive gene expression programs [62], we postulated that induction
357 of PPARGC1A-AT could be implicated in cold-adaptive BA responses involving *Adcy3-at*. Akin
358 to *Adcy3-at*, *Ppargc1a-at* was only induced in thermogenic adipose depots during cold, whereas
359 *Ppargc1a-fl* remained unchanged in all depots investigated (Fig.6c). To test the specific implication
360 of PPARGC1A-AT in *Adcy3-at* expression, we designed two locked nucleic acid inhibitors to
361 silence *(i) Ppargc1a-fl* and *Ppargc1a-at* in combination or *(ii) Ppargc1a-at* in 1°BA. Noteworthy,
362 knocking down *Ppargc1a* did not affect *Adcy3-fl*, but prevented CL316,243 mediated *Adcy3-at*
363 induction (Fig.6d-e), illustrating that PPARGC1A, likely by virtue of truncated PPARGC1A-AT is
364 implicated in *Adcy3-at* transcriptional regulation.
365

366 Finally, to test if cold-inducible ADCY3/PPARGC1A alternative promoter accrual events are
367 conserved in humans, we isolated SVF from deep-neck biopsies of human individuals,
368 differentiated these into human white and brown adipocytes and performed qPCR for full-length
369 and truncated *Ppargc1a* and *Adcy3* transcripts after norepinephrine (NE) stimulation. We observed
370 NE-induced *ADCY3-AT* and *PPARGC1A-AT* expression in brown human adipocytes (Fig.6f,g). We
371 also investigated the broader evolutionary context of *Ppargc1a-at* and *Adcy3-at* by sequence
372 comparison across a panel of thermogenic and non-thermogenic species (Fig.S7c). We found that
373 *Ppargc1a-at* exon 1 was broadly conserved across eutherian species (Fig.6j, Fig.S7d,e), whereas
374 mouse *Adcy3-at* was only conserved within selected rodent species (Fig.S7f) and likely arose
375 independently from human *ADCY3-AT* that was only conserved in primates (Fig.S7g). Despite this
376 convergent ADCY3-AT evolution, rodent and primate *Adcy3-at* transcripts encoded sequence- and
377 structurally related proteins (Fig.6k). Thus, cold stress employs an evolutionarily ancient signal
378 transduction axis that couples truncated PPARGC1A-AT proteins to cold-induced, rheostatic
379 transcriptional responses in activated brown adipocyte that, amongst others, involves ADCY3-AT.
380
381 ***Discussion:***
382 Since the re-discovery of active and recruitable BAT in humans[3-5], enhancing brown fat activity
383 has been increasingly recognized as innovative therapeutic regimen to mitigate obesity and obesity-
384 related health decline. Understanding BAT activity and increasing energy expenditure by ectopic
385 BAT activation can thus become key to control metabolic health in a positive manner. Whilst the
386 molecular circuitry underlying thermogenic activation of brown fat is becoming increasingly well
387 understood, we lack detailed understanding of how BAT activation is kept in balance to avoid
388 negative consequences of exaggerated energy dissipation. Here, we have demonstrated a novel,
389 evolutionary conserved molecular mechanism that functions as a rheostat to maintain BAT
390 function. This is based on the expression of an N-terminally truncated ADCY3-AT isoform that
391 regulates cAMP synthesis during chronic cold exposure and, thereby, maintains BAT energy
392 homeostasis.
393
394 Expression of novel ADCY isoforms has also been demonstrated in other cell types, i.e., vascular
395 smooth muscle cells (VSMCs). A crucial change in VSMC function is the trans-differentiation from
396 a from contractile/quiescent to a secretory/proliferative phenotype, which underlies artherogenesis
397 and vascular remodeling [63]. Trans-differentiation in response to the pro-atherogenic cytokine
398 interleukin-1beta (IL-1b) relies on *de novo* expression of ADCY8 in VSMCs [64, 65]. However, an
399 increase in intracellular cAMP levels is supposed to inhibit the secretory/proliferative VSCM
400 phenotype [66, 67]. Strikingly, the ADCY8 isoforms expressed in VSCMs upon IL-1b stimulation are

splice variants which results in a shorter ADCY8 proteins, which are catalytically inactive. N-terminally truncated ADCY8 proteins act in a dominant-negative manner on other ADCY isoforms by forming heterodimers, retaining them in the ER and reducing intracellular cAMP levels [68, 69]. This is in line with our results, mirroring our observation of a stimulus-dependent *de novo* expression of truncated ADCY3-AT in BAT. Thus, we here delineate that balancing cAMP levels by expressing truncated ADCY isoforms is a more broadly applicable mechanisms that occurs not only in VSCMs but also in thermogenic fat and across different ADCY isoforms. Whether the regulation of *de novo* expression is regulated by common signaling pathways in different cell types, is not known. We here identified a H3K4me3-marked promoter in intron 2 of the *Adcy3* gene, selectively induced upon cold, resulting in novel transcriptional start site for a 5'-truncated *Adcy3* mRNA isoform. The regulation of epigenetic modifications in the context of cAMP signaling is unknown, but it has been shown that the expression of a histone demethylase is controlled by the transcription factor CREB (cAMP-response binding protein), which is activated by cAMP/PKA-dependent phosphorylation [70]. For instance, the beta2-adrenergic receptor agonist Clenbuterol engages cAMP/PKA/p-CREB signaling, which then drives the expression of *Jhdm2a*, a histone demethylase via direct binding of p-CREB to the CRE (cAMP response element) site in the JHDM2a promotor [71]. For ADCY8, *de novo* expression seems to result from both, transcriptional activation and alternative splicing [68]. Strikingly, the mouse *Adcy8* promoter contains a CRE site upstream of the TSS that is required for basal and cAMP-dependent promoter activity [72, 73]. Thus, cAMP-dependent control of *Adcy* isoforms, directly or indirectly by epigenetic modifications, might have emerged as unifying mechanism.

Expression of truncated protein isoforms in metabolically active tissue, like adipose tissue or muscle, is conserved among different proteins that converge in common signaling pathways in a cell-type specific manner. Here, we demonstrated that cold exposure results in the expression of a truncated PPARGC1A-AT proteoform, which contributes to induction of *Adcy3-at* expression. The stimulus that induces *de novo* expression of the truncated proteins can, however, be different yet appropriate towards the seminal function of the tissue, i.e., cold exposure for the thermogenic BAT and endurance training for truncated PPARGC1A isoforms leading to the expression of truncated PPARGC1A isoforms PGC-1a2, 3, or 4[28, 61, 74]. As these stimuli, and the resulting protein expression, are crucial for the function and homeostasis of respective tissues, identifying pharmacological means to target these truncated isoforms is therapeutically relevant. Based on our results from *Adcy3ΔAT* mice, pharmacologically targeting *Adcy3-at* expression could pave the way to re-activate BAT function and thereby mitigate, or even prevent, obesity and obesity-related metabolic decline.

436 ***Figure legends:***

437

438 ***Figure 1: Transcriptional regulation of cAMP biosynthesis during cold adaptation of adipose***
439 ***tissue.*** (**a-c**) Volcano plot of all and significantly altered (cyan, magenta) genes in BAT (**a**, n=2,290;
440 1,086/1,204 up-/downregulated DEGs), iWAT (**b**, n=1,252; 804/448 up-/downregulated DEGs)
441 and eWAT (**c**, n=655 up-/downregulated DEGs) in 20 weeks old C57BL/6N male mice housed at
442 room temperature (22°C) or after 24 h (**a,c**) and 72 h (**b**) of 5°C cold exposure as determined by
443 mRNA-seq. Statistically significant genes were defined as FDR ≤0.05 and log transcripts per
444 million (TPM)>0. n=3-5 animals per temperature condition were analyzed. (**d-f**) KEGG pathway
445 enrichments (Benjamini & Hochberg corrected *P*-value ≤ 0.05) for DEGs shown in (**a-c**). (**g-i**)
446 mRNA expression of adenylyl cyclase isoforms abundance in BAT (**g**), iWAT (**h**) and eWAT (**i**)
447 determined by mRNA-seq and depicted in TPM. Bar graphs represent mean ± SD with all data
448 points plotted and unpaired, two-tailed, and non-parametric Mann-Whitney tests were performed
449 to assess statistical significance. *P*-values are indicated within the panel. **(j-k**) Analysis of single-
450 nucleus RNA-seq (snRNA-seq) data from *Adipoq*-tdTomato positive adipocyte nuclei housed at
451 thermoneutrality (TN), room temperature (RT), and animals after cold exposure (CE) at 8°C for 4
452 days (**j**). The colors depict expression of *Adcy3* (green), *Ucp1* (red) or both (yellow). (**k**) Ridgeline
453 plots depicting frequency (in nuclei) of expression of BAT identity genes at indicated temperatures.

454

455 ***Figure 2: ADCY3 is required for cAMP biosynthesis in BAT and required for cold adaptation in***
456 ***obesity.*** (**a**) Illustration of breeding strategy to obtain adipocyte-specific *Adcy3* knockout mice
457 (*Adcy3-AdcKO*) and *LoxP* controls. (**b**) Quantification of *Adcy3* expression in BAT of chow-diet
458 fed, male *LoxP* (n=4) and *Adcy3-AdcKO* (n=4) by RNA-seq. (**c**) Determination of total cAMP
459 levels by ELISA in BAT obtained from chow-diet fed, male *LoxP* (n=4) and *Adcy3-AdcKO* (n=4)
460 housed at 22°C and plotted as fold-change (fc). (**b-c**) Bar graphs represent mean ± SD with all data
461 points plotted. Unpaired, two-tailed, and non-parametric Mann-Whitney tests were performed to
462 assess statistical significance. *P*-values are indicated within the panel. (**d**) Body weight trajectories
463 in chow diet-fed, male *LoxP* (n=8) and *Adcy3-AdcKO* (n=8) mice. (**e-f**) Blood glucose levels during
464 (**e**) glucose tolerance tests and (**f**) insulin tolerance tests in chow diet-fed, male *LoxP* (n=8) and
465 *Adcy3-AdcKO* (n=8) mice. (**d-f**) Graphs represent mean ± SD with all data points plotted. Statistical
466 significance was determined by performing Two-Way ANOVA with repeated measurements for x
467 values (mixed models). *Post-hoc P*-value correction to account for multiple testing was performed
468 using Bonferroni adjustment. The source of variation, % of the variation and exact *P* values are
469 given in table insets. (**g**) Indirect calorimetric quantification of respiratory Exchange Ratios (RER)
470 in chow-diet fed, male *LoxP* (n=8) and *Adcy3-AdcKO* (n=8) mice. (**h**) Indirect calorimetric

471 measurement of oxygen consumption in chow-diet fed, male *LoxP* (n=8) and *Adcy3-AdcKO* (n=8)
472 mice. (**i**) Quantification of mean daily oxygen consumption in chow-diet fed, male *LoxP* (n=16)
473 and *Adcy3-AdcKO* (n=14) mice. (**j**) Indirect calorimetric determination of mean daily locomotor
474 activity in chow-diet fed, male *LoxP* (n=8) and *Adcy3-AdcKO* (n=8) mice. (**i-j**) Bar graphs represent
475 mean ± SD with all data points plotted and parametric, unpaired, two-tailed Student's t-tests were
476 performed to assess statistical significance. *P*-values are indicated within the panel. (**k**) BW
477 trajectories in HFD-fed, male *LoxP* (n=8) and *Adcy3-AdcKO* (n=8) mice. (**l-m**) Blood glucose
478 levels during (**l**) glucose tolerance tests and (**m**) insulin tolerance tests in HFD-fed, male *LoxP* (n=8)
479 and *Adcy3-AdcKO* (n=8) mice. (**k-m**) Graphs represent mean ± SD with all data points plotted.
480 Statistical significance was determined by performing Two-Way ANOVA with repeated
481 measurements for x values (mixed models). *Post-hoc P*-value correction to account for multiple
482 testing was performed using Bonferroni adjustment. The source of variation, % of the variation and
483 exact *P* values are given in table insets. (**n**) Indirect calorimetric quantification of respiratory
484 Exchange Ratios (RER) in HFD-fed, male *LoxP* (n=8) and *Adcy3-AdcKO* (n=8) mice. (**o**) Indirect
485 calorimetric measurement of oxygen consumption in HFD-fed, male *LoxP* (n=8) and *Adcy3-*
486 *AdcKO* (n=8) mice. (**p**) Indirect calorimetric determination of mean daily locomotor activity in
487 HFD-fed, male *LoxP* (n=8) and *Adcy3-AdcKO* (n=8) mice. Bar graphs represent mean ± SD with
488 all data points plotted and parametric, unpaired, two-tailed Student's t-tests were performed to
489 assess statistical significance. *P*-values are indicated within the panel.
490
491 ***Figure 3: Activated brown adipocytes express a truncated ADCY3 (ADCY3-AT) transcript and***
492 ***protein isoform.*** (**a**) Sashimi plots visualizing splicing junctions from aligned RNA-seq data in
493 BAT in the murine *Adcy3* gene from 22°C-housed 20 weeks old male wildtype C57BL/6N mice or
494 from animals singly housed at 4 °C for a period of 24 h prior to harvesting adipose tissues. Data
495 represent n=3-5 individual mice per condition. *Illu*, Illumina short-read RNA-seq; *Telo*, TeloPrime
496 Full-Length cDNA-seq; *cDNA*, Direct cDNA-seq. Reads were aligned against GENCODE M29
497 annotation and transcript re-assembly using Illumina short-read and full-length RNA-seq using
498 FLAIR[75]. (**b**) Schematic illustration of (1) full-length *Adcy3-fl* transcript and ADCY3-FL protein
499 structure, and (2) *Adcy3-at* transcript and ADCY3-AT protein structure (2). (**c-d**) Expression of
500 *Adcy3-fl* (**c**) and *Adcy3-at* (**d**) in BAT of chow diet-fed animals housed at 22°C (n=4 *LoxP*, n=4
501 *Adcy3-AdcKO*) and 5°C (n=3 for *LoxP*, n=3 for *Adcy3-AdcKO*) determined by RNA-seq. (**e-g**)
502 Relative expression of *Adcy3-fl* and *Adcy3-at* as determined by quantitative PCR analysis of BAT
503 (**e**), iWAT (**f**) and eWAT (**g**) of male C57BL/6N mice housed at room temperature (n=3) or exposed
504 to 5°C for 24 h (n=3). (**h-j**) Relative expression of *Adcy3-fl* and *Adcy3-at* as determined by
505 quantitative PCR analysis of primary adipocytes derived from stromal-vascular fraction (SVF) cells

506 isolated from BAT (**h**), iWAT (**i**), and eWAT (**j**) depots and stimulated with 6 h of 10 µM
507 CL316,243. Replicates represent primary adipocytes isolated from individual mice (n=3 mice per
508 depot and stimulation regimen). (**c-j**) Bar graphs represent mean ± SD with all data points plotted.
509 To test for statistical significance, non-parametric (ranked) Kruskal–Wallis one-way analysis of
510 variance (ANOVA) tests with Dunn's correction for multiple testing were performed. *P*-values are
511 indicated in the panel. (**k-l**) Immunoblot analysis of primary adipocytes differentiated from SVF
512 cells isolated from BAT (1°BA) and iWAT (1°iWA), stimulated for 6 h and 24 h with 1 mM db-
513 cAMP (cAMP) and 10 µM CL316,243 (CL) and blotted using pan anti-ADCY3 antibody. Bands
514 corresponding to ADCY3-FL and ADCY3-AT are from the same membrane but represent diffent
515 exposure times. Calnexin (CLNX) was used as loading control.
516
517 ***Figure 4: ADCY3-AT inhibits oxidative metabolism in vitro and in vivo.*** (**a**) Illustration of
518 CRISPR-Cas9 mediated excision of *Adcy3-at* specific exon 2b including *Adcy3-at* TSS (light blue)
519 yielding ADCY3-AT specific knockout mice. (**b-c**) Relative expression of (**b**) *Adcy3-at* and (**c**)
520 *Adcy3-fl* determined by qPCR analysis of BAT, iWAT, and eWAT of chow diet fed, male *LoxP*
521 and *Adcy3*Δ*AT* mice housed at 22°C (n=3-4 per tissue and genotype). Bar graphs represent mean ±
522 SD with all data points plotted. An unpaired, two-tailed, and non-parametric Mann-Whitney tests
523 were performed to assess statistical significance. *P*-values are indicated within the panel. (**d**) Body
524 weights in chow diet-fed, male *LoxP* (n=7) and *Adcy3*Δ*AT* (n=9) mice. (**e**) Blood glucose excursion
525 during glucose tolerance test in chow diet-fed, male *LoxP* (n=7) and *Adcy3*Δ*AT* (n=9) mice. (**f**)
526 Cumulative food intake as measured by indirect calorimetry in chow diet-fed, male *LoxP* (n=7) and
527 *Adcy3*Δ*AT* (n=9) mice. (**g**) Indirect calorimetric measurement of oxygen consumption in chow-diet
528 fed, male *LoxP* (n=7) and *Adcy3*Δ*AT* (n=9) mice. (**d-g**) Graphs represent mean ± SD with all data
529 points plotted. Statistical significance was determined by performing Two-Way ANOVA with
530 repeated measurements for x values (mixed models). *Post-hoc P*-value correction to account for
531 multiple testing was performed using Bonferroni adjustment. The source of variation, % of the
532 variation and exact *P* values are given in table insets. (**h-i,l**) Relative expression of indicated
533 mRNAs in (**h**) chow diet-fed, male *LoxP* (n=5 for 22°C, n=6 for 5°C) and *Adcy3*Δ*AT* (n=3 for
534 22°C, n=4 for 5°C), (**i**) chow diet fed, male *LoxP* (n=3) and *Adcy3*Δ*AT* (n=3) and (**l**) HFD-fed, male
535 *LoxP* (n=3) and *Adcy3*Δ*AT* (n=3) mice. Bar graphs represent mean ± SD with all data points plotted
536 and unpaired, two-tailed, non-parametric Mann-Whitney tests were performed for indicated
537 comparisons to assess statistical significance. *P*-values are given within the panel. (**j**) BW in 16 to
538 19 weeks old, HFD-fed male *LoxP* (n=4-5) and *Adcy3*Δ*AT* (n=4-6) mice. (**k**) Blood glucose during
539 glucose tolerance tests in HFD-fed, male *LoxP* (n=4) and *Adcy3*Δ*AT* (n=4) mice. (**j-k**) Graphs
540 represent mean ± SD with all data points plotted. Statistical significance was determined by

541 performing Two-Way ANOVA with repeated measurements for x values (mixed models). *Post-*
542 *hoc P*-value correction to account for multiple testing was performed using Bonferroni adjustment.
543 The source of variation, % of the variation and exact *P* values are given in the table insets. (**m,n**)
544 Oxygen consumption rates (**m**) and extracellular acidification rates (**n**) in 1°BA derived from SVF
545 of *LoxP* or *Adcy3ΔAT* mice after stimulation with 10 µM CL316,243. The numbers of measured
546 wells are indicated in the panel. (**o-p**) Oxygen consumption rates (**o**) and extracellular acidification
547 rates (**p**) in 1°BA derived from SVF of *LoxP* or *Adcy3ΔAT* mice. OM, oligomycin; FCCP, AA,
548 Antimycin A; Rot, Rotenone. The numbers of measured wells are indicated in the panel. (**m-o**)
549 Graphs represent mean ± SD with all data points plotted. Statistical significance was determined
550 by performing Two-Way ANOVA with repeated measurements for x values (mixed models). *Post-*
551 *hoc P*-value correction to account for multiple testing was performed using Bonferroni adjustment.
552 The source of variation, % of the variation and exact *P* values are given in the table insets.
553
554 **Figure 5: ADCY3-AT alters ADCY3 subcellular localization and thereby limits cAMP**
555 **biosynthesis. (a**) Co-immunoprecipitation of ADCY3-AT-FLAG and ADCY3-FL-HA in CHO
556 cells. CHO K1 cells stably expressing ADCY3-FL-HA were transiently transfected with mCherry
557 (upper row) or ADCY3-AT-Flag (bottom row). Total protein lysates were incubated with anti-
558 FLAG magnetic beads and the different fractions were analyzed by Western blot (Input, NB: non-
559 bound, W: wash, Eluate). (**b**) Quantification of Western blot analyses. The ratio of ADCY3-FL-
560 HA protein density in the eluate of total protein lysates described in (**a**). Bar graphs represent mean
561 ± SD with all data points plotted. An unpaired, two-tailed, and non-parametric Mann-Whitney tests
562 were performed to assess statistical significance. If relevant, *P*-values are indicated within the
563 panel. (**c**) Biotinylation assay. Representative Western blot analysis of total protein lysates isolated
564 from CHO cells stably expressing CNGA2-TM (+, CNB-3B10), transiently transfected with
565 mCherry (-, anti-RFP antibody), or stably expressing ADCY3-FL-HA or ADCY3-AT-HA (anti-
566 HA antibody). Cells were treated with the biotinylation reagent Sulfo-NHS-SS-Biotin, lysed
567 (Input), and purified using a NeutrAvidin-agarose-resin (F: flow through, W: wash, E: eluate, B:
568 beads). (**d**) Quantification biotinylation assay. Densitometric analysis of n=3 (CNGA2-TM,
569 mCherry, ADCY3-FL-HA) and n=4 (ADCY3-AT-HA) Western blots shown in (**e**). Values were
570 normalized to the respective input sample. The ratio of eluate to input in % is shown as mean ± SD
571 with all data points plotted. To test for statistical significance, non-parametric (ranked) Kruskal–
572 Wallis one-way analysis of variance (ANOVA) tests with Dunn's correction for multiple testing
573 were performed. *P*-values are indicated in the panel. (**e**) CHO cells stably expressing ADCY3-FL-
574 HA and transiently transfected with mCherry-CAAX were sonicated and labeled with an anti-
575 Calnexin antibody (ER-marker, magenta) and an anti-HA antibody (green). mCherryCAAX

576 fluorescence is indicated in red. Single channels are shown at the top, merged images at the bottom
577 row. White boxes are shown as magnified view at the bottom-right. Arrows point to endoplasmic
578 reticulum-plasma membrane (ER-PM) contact sites, asterixis indicate contact-free parts within the
579 membrane sheet. Scale bar: 10 µm. (**f**) See (**e**) for CHO cells stably expressing ADCY3-AT-HA.
580 (**g**) Representative Western blot analysis of total protein lysates isolated from CHO K1 cells stably
581 expressing ADCY3-FL-HA or, transiently expressing (*top*) mCherry or (*bottom*) ADCY3-AT-
582 FLAG-2A-mCherry. Cells were treated with the biotinylation reagent Sulfo-NHS-SS-Biotin and
583 the protein lysate was purified using a NeutrAvidin-agarose-resin. The following samples were
584 loaded: Input, Flow-through (F), Wash (W1-3), Eluate, Beads (B). The presence of Adcy3-FL-HA
585 in the plasma membrane was verified using an anti-HA antibody, an anti-mCherry antibody was
586 used as a control. (**h**) AlphaFold modeling of ADCY3-FL/ADCY3-AT heterodimer complex. Full-
587 colored and transparent domains depict non-conserved and conserved residues between ADCY3-
588 FL and ADCY3-AT, respectively.
589
590 **Figure 6: Conserved and cold-inducible PPARGC1A-AT drives *Adcy3-at* expression in brown**
591 **adipocytes. (a)** Sashimi plots visualizing splicing junctions from aligned RNA-seq data in BAT in
592 the murine *Ppargc1a* gene locus from 22°C-housed 20 weeks old male wildtype C57BL/6N mice
593 or animals singly housed at 4 °C for a period of 24 h prior to harvesting adipose tissue. n=3-5
594 animals per temperature. *Illu*, Illumina short-read RNA-seq; *Telo*, TeloPrime Full-Length cDNA-
595 seq; *cDNA*, Direct cDNA-seq. Reads were aligned against GENCODE M29 annotation and
596 transcript re-assembly using Illumina and ONT information using FLAIR[75]. (**b**) Illustration of full-
597 length *Ppargc1a-fl* transcript and PPARGC1A-FL protein structure (1) as well as *Ppargc1a-at*
598 transcript and PPARGC1A-AT protein structure (2). (**c**) Relative expression of *Ppargc1a-fl* and
599 *Ppargc1a-at* as determined by quantitative PCR analysis of primary adipocytes derived from
600 stromal-vascular fraction (SVF) cells isolated from BAT (*left*), iWAT (*middle*), and eWAT (*right*)
601 depots. Replicates represent primary adipocytes isolated from individual mice (n=3 mice per
602 adipose depot and stimulation regimen). Bar graphs represent mean ± SD with all data points
603 plotted. To test for statistical significance, non-parametric (ranked) Kruskal–Wallis one-way
604 analysis of variance (ANOVA) tests with Dunn's correction for multiple testing were performed.
605 *P*-values are indicated in the panel. (**d-e***) Adcy3* (**d**) and *Ppargc1a* (**e**) isoform expression in 1°BA
606 after transfection with 25 nM scrambled (scr LNA) or *Ppargc1a* locked nucleic acids (LNAs)
607 targeting both *Ppargc1a* (*Ppargc1a-at_fl* LNA) isoforms or Ppargc1a-at exclusively (*Ppargc1a-at*
608 LNA) knockdown. Data represent three to four independent experiments, each performed in three
609 technical replicates. Paired samples are represented by individual lines and scr LNA set to unity
610 =1. Line graphs represent mean ± SD with all data points plotted and paired, two-tailed Student's

611 T-tests were performed to assess statistical significance. *P*-values are indicated within the panel. (**f-**
612 **i**) Expression of human *ADCY3-AT* (**f**) and *PPARGC1A-AT* (**g**) in primary human brown adipocytes
613 (hBA) derived from stromal-vascular precursors and stimulated with 1 μM norepinephrine (NE)
614 for 16 h as described previously[76]. (**h**) Genomic conservation of *Ppargc1a-at* among representative
615 mammals. Color gradient indicates percent nucleotide identity of exon 1b relative to mouse.
616 Phylogeny based on [77]. (**i**) Overlap of predicted structure (AlphaFold) of mouse and human
617 ADCY3-AT proteins. Cyan and Gold depict mouse and human isoform, respectively

618 ***Methods:***

619 *Animal care and research diets:*

620 Experimental animals were kept in individually ventilated cages (IVC Type II long) in a pathogen-
621 free (SPF) animal facility with controlled temperature (22-24 °C), light/dark cycle (12h/12h) and
622 humidity (50-70%). Care of animals was within institutional and animal-care committee guidelines
623 approved by (1) local (Bezirksregierung Köln) or regional (Tierschutzkommission acc. §15 TSchG
624 of Landesamt for Natur, Umwelt und Verbraucherschutz (LANUV) North-Rhine Westphalia,
625 Germany) authorities, internal accession no. 84-02.04.2017.A009 or (2) Ministry of Environment
626 of Denmark (Miljø- og Fødevarestyrelsen), internal accession no. 2018-15-0201-01562. All
627 animals were maintained and regularly backcrossed to a C57BL/6N background and housed in
628 groups of 3-4 animals per cage and had *ab libitum* access to food and drinking water. All mice were
629 sacrificed by cervical dislocation or carbon dioxide asphyxiation. Unless otherwise indicated,
630 animals were allowed ad libitum access to chow diet (ssniff® R/M-H Low-Phytoestrogen, V1554)
631 containing 62 kJ% carbohydrates, 27 kJ% protein and 11 kJ% fat and drinking water. Diet-induced
632 obesity (DIO) was achieved by feeding a high-fat diet (HFD, D12492 (I) mod; Sniff) containing 22
633 kJ% carbohydrates, 24k J% protein and 54 kJ% fat from starting at 6-8 weeks of age.

634

635 *Mouse husbandry:*

636 *Adcy3* floxed mice were kindly provided by Chen and colleagues [24]. Herein, exon 3 of the *Adcy3*
637 gene is flanked by two intronic *LoxP* sites, each 75 base pairs upstream or downstream of the exon.
638 Deleting exon 3 of *Adcy3* causes a frame shift mutation, resulting in a premature stop codon within
639 the *Adcy3* gene. Adipose tissue-specific deletion of both, *Adcy3-fl* and *Adcy3-at*, isoforms of *Adcy3*
640 was achieved using cre recombinase-mediated excision of *LoxP*-flanked ('floxed') gene sequences.
641 For this, mice floxed for *Adcy3* ($Adcy3^{LoxP/LoxP}$) were interbred with mice expressing the *Adipoq*-
642 cre recombinase under control of mature adipocyte specific *Adipoq* promote ($Adipoq\text{-}cre^{+/}$cre) [36].
643 *AdipoQ*-Cre mice were obtained from Jax (Stock no. #010803) and backcrossed to C57BL/6N for
644 at least five generations. Resulting ($Adcy3^{LoxP/LoxP}$, $Adipoq\text{-}cre^{+/cre}$ mice (*Adcy3-AdcKO*) were
645 compared to ($Adcy3^{LoxP/LoxP}$, $Adipoq\text{-}cre^{+/+}$) littermates as controls (*LoxP*).

646

647 *Generation of Adcy3ΔAT mice:*

648 *Adcy3ΔAT* knock-out ES cells were generated using CRISPR/Cas9 technology using a modified
649 pX330 plasmid vector [78, 79] containing two gRNAs and a GFP-puromycin selection cassette. The
650 plasmid was kindly provided by Dr. Stefan Frank and was constructed at the Max-Planck Institute
651 for Molecular Biomedicine (Münster, Germany). The knock-out strategy targeted 978 bp deletion
652 of *Adcy3-at* starting exon ('exon 2b') and flanking regions from *Adcy3* genomic DNA. A CRISPR

653 design online tool (http://crispr.mit.edu/) was used to generate *Adcy3-AT* specific single guide RNA
654 (sgRNA) sequences. The list of sgRNAs and primers for generation of *Adcy3*ΔAT mice are given
655 in Supplementary table S3. The quality score of the design pipeline represents the reliability of an
656 on-target activity computed as 100%, minus a weighted sum of off-target hit-scores. A chosen
657 gRNA with a high-quality score was cloned into the BbsI-digested pX330 vector, followed by the
658 second gRNA, which was cloned using a SapI-mediated Golden Gate assembly method for the
659 concatemerization of gRNA cassettes.
660
661 *Vector generation:*
662 For CRISPR/Cas9 construct generation, 1 µg of the pX330 vector was enzymatically digested with
663 FastDigest BbsI (Thermo Fisher Scientific) for 30 min at 37 °C. The digested vector was purified
664 using the MinElute PCR Purification kit (Qiagen) following the manufacturer's instructions. gRNA
665 was phosphorylated by a T4 polynucleotide kinase according to product instructions (New England
666 Biolabs). For the amplification of phosphorylated sgRNA it was incubated with 1 µl of forward and
667 reverse primers (100 µM, Supplementary Table S3) for 30 min at 37 °C. Annealing was performed
668 at 95 °C for 5 min and subsequently the reaction was cooled to 25 °C at a cooling rate of 5 °C/min.
669 1 µl of the oligo reaction was ligated with 50 ng of digested pX330 vector and was assessed using
670 the Quick Ligase kit (New England Biolabs) for 20 min at room temperature according to the
671 manufacturer's instructions. Plasmid Safe DNase kit (EpiCentre) was used to degrade any
672 unspecific recombination products for 30 min at 37 °C, following the instructions of the kit.
673
674 *Culturing mouse embryonic fibroblasts and ES cells and ES cell transfection:*
675 Mouse embryonic fibroblasts (EF) were used as feeder cells for mouse embryonic stem cells (ESC).
676 EF cells were passaged before reaching full confluence and EF-cell medium was changed to fresh
677 medium every two days. To obtain mitotically inactive fibroblasts, cell growth was stopped by
678 adding 10 µg/ml MMC after three generations (EF3) and the reaction was incubated for another 2-
679 4 h. MMC was removed, and cells were rinsed with 1xPBS. The cells were afterwards stored by
680 freezing or directly used for seeding. To seed MMC-treated EF3 cells, tissue culture dishes were
681 gelatinized with 0.2% gelatin in advance to enhance the attachment of MMC-treated cells to the
682 dish-surface. ES cells were cultivated on top of MMC-treated EF3 cells and ES cell culture medium
683 was exchanged every day. ES cells were passaged to new culture plates or were frozen for long
684 term use and to maintain pluripotency.
685
686 10^7 ESC were mixed with 40 µg of the CRISPR construct dissolved in PBS, resuspended in 400
687 µL transfection buffer (RPMI without Phenol Red, Gibco, Karlsruhe, Germany), and mixed with

688 the plasmid construct DNA. The total volume was adjusted to 800 µl. Transfection was achieved
689 by electroporation at 450 µFD and 240 V at room temperature (Gene Pulser Xcell, Bio-Rad
690 Laboratories GmbH, München, Germany) in a 4 mm electroporation cuvette. The time constant
691 was set to around 7-10 seconds. After 5 min incubation, cells were resuspended in ES-cell medium,
692 diluted 1:20000 and plated on a gelatinized 10 cm culture dishes with previously prepared MMC-
693 treated EF3 cells. Following two days of incubation in ES-medium, single clones were transferred
694 to three 96-well plates and selected via colony PCR. In addition to PCR confirmation, Southern
695 blot analysis was used to confirm the deletion of *Adcy3-AT* as explained below. Validated colonies
696 were transferred in 40 µl PBS to a 96-well (round-bottom) plate containing 25 µl trypsin.
697 Trypsinization took place for 5 min at 37 °C and the reaction was stopped by adding 100 µl ES-
698 medium. Cell suspension for each colony was added up to 15 mL with ESC-medium and seeded in
699 one separate 10 cm dish per colony. To achieve higher homogeneity among targeted ESC
700 populations, positive colonies were again seeded out after expansion in three 96-well plates each
701 and selection by PCR and Southern blot repeated. Positive colonies were trypsinized and seeded
702 on 10 cm dishes for expansion as before.
703
704 *Generation of Adcy3ΔAT chimeric mice from genetically modified ESC clones and genotyping:*
705 Positive *Adcy3ΔAT* clones were injected into donor blastocysts, which was performed by Taconic
706 Biosciences (Cologne, Germany). Injected blastocysts were implanted into pseudo-pregnant foster
707 mice and resulting progenies (Generation F1) partly develop from cells derived from the *Adcy3*ΔAT
708 ESC. Male chimeric F_1 mice were backcrossed to C57BL/6N mice to produce the F_2 generation.
709 Germline transmission was confirmed by PCR and Sanger sequencing of DNA extracted from the
710 tails of F_2 mice. Genotyping protocols for the *Adcy3ΔAT* transgenic allele was conducted using the
711 following primers which were also used for genotyping from mouse tail DNA:
712 *Adcy3ΔAT*_E2B_F_1: 5'-GGGACTGAGGGAGCCTAAGA-3'
713 *Adcy3ΔAT*_E2B_R: 5'-GGCCAGGTTACATGAGGACA-3'
714 *Adcy3ΔAT*_E2BF_2_R2: 5-'-GGAGAGCTTCGAGTGTGTCAAG-3'.
715
716 *Southern blot of Adcy3ΔAT embryonic stem cells:*
717 For confirmation of *Adcy3-at* deletion in ESC, genomic DNA (5-10 µg) derived from transfected
718 ESC was digested by high concentrated HindIII-HF or high concentrated BamHI-HF (NEB). In all
719 Southern blot analyses, wildtype Bruce 4 (Br4) ESC DNA was used as negative control. Overnight
720 digested DNA was loaded with loading dye onto a 0.8 % agarose gel and separated at 30 V for at
721 least 16 hours. The DNA was consequently de-purinated within the gel by incubating the gel in
722 0.25 M HCl for 20 min under continuous shaking. DNA was then transferred into a charged

723 Amersham Hybond-XL nylon membrane by alkaline capillary transfer using a sodium hydroxide
724 solution (0.4 M NaOH) and the membrane was incubated in 2X SSC for 20 min and finally dried
725 at 80 °C for 45 min to fix the DNA on the membrane. To probe for the modified *Adcy3*Δ*AT* allele,
726 a 394 bp probe was amplified from Bruce4 ESC genomic DNA with primers 5'-
727 ATCCTGTGCTGACATGGGTG-3' and 5'-AATTCCCCACTGACCAACGG-3' using high-
728 fidelity PCR Master Kit. The extracted probes were radioactively labeled with 2.5 µl [alpha-32P]
729 dCTP (Amersham) according to the instructions of the kit (LaddermanTM Labeling Kit, Takara).
730 The probe was mixed with 100 µl TE buffer (10mM, pH8.5) and purified via spin-column
731 chromatography using Illustra MicroSpin S-200 HR columns. The dried membrane was incubated
732 in 2X SSC buffer to prepare for pre-hybridization. Pre-hybridization was performed in pre-
733 hybridization buffer (1 M sodium chloride, 50 mM Tris-CL pH 7.5, 10 % Dextran sulfate, 1% SDS,
734 250 µg/ml salmon sperm DNA) at 65 °C for at least 4 h. After pre-hybridization radioactively
735 labeled probes were added to the membrane and the reaction was incubated overnight at 65 °C.
736 After several washing steps, the membrane was placed in direct contact with Kodak MS
737 hypersensitive films for 4-24 h to detect the radioactive signal. Expected product sizes were 4.75
738 kb for *Adcy3* wildtype and 3.75 kb for *Adcy3*Δ*AT* constructs.
739
740 *Plasmid vector cloning:*
741 Overexpression constructs (ADCY3-AT, 3201 bp and ADCY3-FL, 3792 bp) were PCR amplified
742 from synthetic oligonucleotides by Thermo Fischer scientific. The DNA fragment was inserted into
743 pcDNA3.1(+) vector backbones using NheI / XhoI restriction enzymes. For ADCY3-AT the first
744 ATG in-frame within exon 2 was used as start codon. Sequences encoding Kozak sequences
745 (GCCACC) and a 295 bp artificial intron sequence were included upstream of ATG. To generate
746 pc3.1(+)-mADCY3-AT-FLAG, the FLAG tag was added by PCR and the coding sequence cloned
747 into the vector backbone using EcoRI/XhoI. Additional details on cloning procedures are available
748 upon reasonable request.
749
750 *Illumina and Nanopore RNA sequencing and data analysis:*
751 Paired end libraries were constructed using the NEBNext Ultra II RNA Library Prep Kit (New
752 England Biolabs, Ipswich, MA, USA) following the manufacturer's protocol and sequenced on a
753 NovaSeq 6000 (Illumina, San Diego, CA, USA) in 2x50-bp paired-end reads. Transcriptional
754 expression was quantified using Salmon[80] by mapping RNA-seq reads to the ENSEMBL m38
755 (mm10) transcriptome. Adcy3-at transcript identified in the de novo ONT/Illumina transcriptome
756 assembly (see section below), was added to the ENESEML m38 transcriptome and counted as an
757 independent gene. Transcript counts were imported and summarized to ENSEMBL genes IDs using

758 tximport[81] and differential expression analyses were conducted with edgeR [82]using glmQLFTest.
759 KEGG pathway enrichment analyses were conducted using clusterProfiler package for R[83].
760
761 *Nanopore RNA-Sequencing and data processing:*
762 RNA was isolated by phenol chloroform extraction and alcohol precipitation followed by two
763 consecutive rounds of poly-A selection using oligo(dT) beads (GenElute mRNA Miniprep Kit,
764 Sigma MRN10) following the manufacturer's recommendations. Subsequently, RNA was alcohol
765 precipitated using NaAcetate and glycogen following the protocol from the Ribo-Zero rRNA
766 Removal Kit (Illumina). Nanopore sequencing libraries were prepared using the TeloPrime Full-
767 Length cDNA Amplification Kit (Lexogen, Austria), the SQK-DCS109 direct cDNA sequencing
768 kit (Oxford nanopore technologies, ONT) and the SQK-RNA002 direct RNA sequencing kit (ONT)
769 according to manufacturer's protocols. Sequencing was performed using FLO-MIN106 R9 flow
770 cells on the GridION platform (ONT). Reads were mapped against the murine genome
771 (GRCm38.p6) using minimap2 [84] and transcriptomes reassembled using FLAIR [75]. Tracks were
772 visualized using gviz [85].
773
774 *Single-nucleus RNA-Sequencing (snRNA-seq) data processing:*
775 Pre-processed data from snRNA-seq from 10X sequencing of mouse 1°BA housed at room-
776 temperature, cold-exposure and/or thermoneutrality was adopted from Sun[34] (ArrayExpress using
777 accession code E-MTAB-8562. Data was normalized (SCTransform), analyzed and plotted using
778 Seurat 4.0.1 package for R[80-83, 86].
779
780 *Chromatin Immunoprecipitation (ChIP) coupled to sequencing (ChIP-seq) and ChIP-qPCR:*
781 Prior to ChIP-seq, brown adipose tissue was dissociated using a gentleMACS Dissociator (Miltenyi
782 Biotec, Germany). The cell suspension was crosslinked with 1 % formaldehyde for 10 min at RT
783 and the reaction was quenched with 0.125 M glycine for 5-10 min at RT. Cells were washed 2X
784 with cold PBS and PMSF and snap-frozen in liquid nitrogen before storing at -80°C. For histone
785 posttranslational modification (PTM) sequencing, BAT of two mice were used and steps performed
786 on ice. First, frozen pellets were thawed on ice for 30-60 min. Pellets were resuspended in 5 ml
787 LB1 (50 mM Hepes, 140 mM NaCl, 1 mM EDTA, 10 % Glycerol, 0.5 % NP-40, 0.25 % Triton X-
788 100) by pipetting and then rotated vertically at 4°C for 10 min. Pellets were centrifuged for 5 min
789 at 1350 x g at 4°C (GH-3.8 rotor = 2400 rpm) and supernatant was aspirated. Pellets were
790 resuspended in 5 ml LB2 (10 mM Tris, 200 mM NaCl, 1 mM EDTA, 0.5 mM EGTA) and incubated
791 at vertical rotation and at room temperature for 10 min. Samples were centrifuged for 5 min at 1350
792 x g at 4°C and supernatant was carefully aspirated. Then, samples were resuspended in 3 ml LB3

793 (10 mM Tris, 100 mM NaCl, 1 mM EDTA, 0.5 mM EGTA, 0.1 % Na-Deoxycholate, 0.5 % N-
794 lauroylsarcosine) and were separated into 2 x 1.5 ml in 15 ml polypropylene tubes, in which they
795 were sonicated with the following settings by Bioruptor Plus sonication: Power = high, 'on' interval
796 = 30 sec, 'off' interval = 45 sec, total time = 10 min (18 cycles of 'on'/'off'). Sonicated samples
797 were transferred to a 1.5 ml microfuge tube and were centrifuged for 10 min at 16000 x g at 4°C to
798 pellet cellular debris. 10 % of sample solution were stored to be used as input control, while the
799 rest was used for ChIP. To capture different H3K4me3 modifications, 3 µl of anti-H3K4me3
800 antibodies (Active Motif, cat. No 39159) were added to the sonicated ChIP reaction and rotated
801 vertically at 4° C overnight. The next day, 100 µl Dynabeads (Protein A or Protein G) for each
802 ChIP sample were prepared according to the manufacturer's instructions, mixed with 1 ml of
803 antibody-bound chromatin, and rotated vertically at 4°C for at least 2-4 hours. Bound beads were
804 washed at least five times in 1 ml cold RIPA and once in 1 ml cold TE buffer containing 50 mM
805 NaCl. Samples were eluted for 15 min with elution buffer at 65°C and continuously shaken at 700
806 rpm. Beads were separated using a magnet and 200 µl supernatant were transferred to fresh
807 microfuge tubes. Previously stored input samples were thawed and mixed with 300 µl Elution
808 buffer. ChIP/input samples were incubated at 65°C in a water bath overnight to reverse the
809 crosslinking reaction. On the third day, 1 volume TE buffer was added at room temperature to dilute
810 SDS in both ChIP and input samples. For digestion of RNA and protein contamination, RNase A
811 was added to the samples and incubated in a 37°C water bath for 2 hours; then proteinase K was
812 added to a 0.2 mg/ml final concentration and incubated in a 55°C water bath for 2 hours. Finally,
813 DNA was extracted using a standard phenol-chloroform extraction method at room temperature
814 and DNA concentrations were measured using a NanoDropTM ND-1000 spectrophotometer or
815 QubitTM dsDNA HS Assay Kit and stored at -80 °C until sequencing or ChIP-qPCR.
816
817 H3K4me3-immunoprecipitated genomic DNA was diluted 1:100 and Chip-qPCR performed with
818 a Light Cycler 480II machine (Roche) using technical duplicates and ChIP-qPCR signals were
819 calculated as % of input. Standard deviations were calculated from technical duplicate reactions
820 and represented as error bars. Quantitative PCR primer sequences were:
821 *Adcy3-fl* TSS_F: 5'-GATGGACTTCCACGAGGCTG-3'
822 *Adcy3-fl* TSS_R: 5'-TACTTCCTTTCCCCCACCCA-3'
823 *Adcy3-at* TSS_F: 5'-GGAGAGCTTCGAGTGTGTCAAG-3'
824 *Adcy3-at* TSS_R: 5'-GTCTCACCTTAAGGCTCCTCCT-3'
825 *Adcy3 exon 3*_F: 5'-CTGTGCCAGATTGTCTCCGT-3'
826 *Adcy3 exon 3*_R: 5'-GTCATGGACTTGGGCTTCCA-3'
827

828 *Mouse tissue RNA isolation:*
829 RNA from indicated tissues and primary brown and inguinal white adipocytes was isolated using
830 Trizol® according to manufacturer's protocols for total RNA isolation.
831
832 *CHO K1 cell culture:*
833 CHO K1 WT cells (ATCC, #CCL-61) were maintained in F-12 Nut Mix + GlutaMAX (#31765-
834 027, Thermo Fisher) at a subconfluent level and passaged every 4 days. Cells stably expressing
835 ADCY3-FL-HA were kept in medium containing 0.8 mg/ml Geneticin (G418 Sulfate, Gibco).
836
837 *Isolation of depot-specific stromal-vascular fraction (SVF) derived 1° adipocytes:*
838 Inguinal white and intrascapular brown adipose tissues from 6-8 weeks-old male mice were
839 dissected after carbon dioxide asphyxiation, minced, and digested with collagenase II (2 mg/mL),
840 DNAse I (15 kU/mL), Dispase II (for BAT: 1.5 mg/mL) and 3.4 % BSA supplemented serum-free
841 SVF culture media Dulbecco's Modified Eagle Medium:Nutrient Mixture F-12 (DMEM/F-12) pre-
842 supplemented with 1 % P/S, 0.1 % Biotin and 0.1 % pantothenic acid. Minced tissues incubated in
843 37 °C shaker at 120 rpm/min for 45 minutes and pipetted in every 15 minutes until the minced
844 tissue particles were completely dissolved. SVF fraction cells were enriched in the pellet of the
845 tubes by sequential filtering and washing steps with 250 μm and 70 μm sterile cell strainers in 10
846 % FBS supplemented SVF culture media. Enriched SVF cells seeded in 6-well plate wells (1
847 well/mice) with 20% FBS supplemented SVF culture media and incubated in cell culture incubator
848 for the required amount of time to enable expansion of the culture.
849
850 *Induction of SVF adipogenesis:*
851 iWAT and BAT depot-specific stromal vascular fraction (SVF) at 80 % confluency were induced
852 for adipogenic differentiation with induction cocktail (1 μM Rosiglitazone, 850 nM Insulin, 1 μM
853 Dexamethasone, 250 μM IBMX, and, for only BAT, 125 μM Indomethacin and 1 nM T3) in 10 %
854 FBS supplemented SVF culture media. After incubation for 2 days with induction media, culture
855 media replenished with the differentiation media (1 μM Rosiglitazone, 850 nM Insulin and for only
856 BAT with 1 nM T3 in 10 % FBS supplemented culture media) on days 2, 4, and 6. Cells were
857 treated with compounds (10 μM CL-316,243; 2 μM Forskolin) on day 7 for and harvested the same
858 day after compound stimulations.
859
860 *LNA-mediated gene knockdown in primary adipocytes:*
861 For transfection of LNA GapmeRs in 1°BA and 1°iWA, 80,000 cells were seeded per well in 6-
862 well plates and grown to confluence in growth medium. Immediately before transfection, medium

863 was changed to fresh differentiation medium without antibiotics. In the meantime, antisense LNA
864 GapmeRs (Exiqon A/S) were diluted to the concentration of 100 nM in OptiMEM and transfected
865 using Lipofectamine® 2000 according to the manufacturer's instructions. LNA sequences are
866 provided in Supplementary Table S5.
867
868 *AAV-mediated cre transduction in primary adipocytes:*
869 On day 4 of iWA and BA differentiation, committed adipocytes were trypsinized, counted and
870 seeded into multi well plates with the experimental setup (180.000 cells / cm^2 growth area) with
871 the differentiation media containing AAV viruses. Primary adipocytes were transduced with
872 AAV8-CMV-Cre (pENN.AAV.CMVs.Pl.Cre.rBG, Addgene #105537-AAV8 Cre) and AAV8-
873 CMV-eGFP (pAAV.CMV.PI.EGFP.WPRE.bGH, Addgene #105530-AAV8 eGFP) viruses with
874 the amount of 100. 000 MOI. Virus containing media replenished on day 6 with fresh differentiation
875 media and cells were treated with compounds (10 µM CL-316,243) on day 7 for and harvested the
876 same day after compound stimulations.
877
878 *Determination of oxygen consumption rates and measurement of glycolytic activity:*
879 *Adcy3-at* deficient SVFs from indicated adipose depots of transgenic mice were seeded into Agilent
880 Seahorse XFe96 Bioanalyzer microplates. Per well, 50,000 cells were seeded and incubated in
881 DMEM/Ham's F-12 medium plus 10 % Fetal Calf Serum, 1 % P/S, 0.1 % Biotin and 0.1 %
882 Pantothenic acid (Growth medium) at 37° C and 5 % CO2 at a standard incubator until confluency
883 is reached. To induce commitment of SVFs into mature adipocytes within Xfe96 microplates,
884 freshly prepared 0.05 % Insulin, 0.005 % Dexamethasone, 0.001 % Rosiglitazone and 0.05 %
885 IBMX (1°iWA) or 0.1 % Indomethacin, 0.001 % Triiodothyronine (1°BA) in growth medium
886 (induction medium) were added. After 48 h of induction, differentiation was initiated using freshly
887 prepared 0.001 % Rosiglitazone (1°iWA) or 0.001 % Triiodothyronine (1°BA) in growth medium
888 (differentiation medium). Differentiation was achieved after 3-4 days of incubation in the
889 differentiation medium. For each seahorse plate the corresponding calibration plate was prepared
890 24 h prior to experiments using 200 µl XF Seahorse Calibrant Agilent per well. The plate was
891 incubated for 24 h in a non-CO2 incubator at 37° C and the instrument set to 37° C 24 h prior to
892 the experiment. One hour before measurements, plates were washed with 1xPBS and the medium
893 changed according to the corresponding experiment analyte kits (MitoStressKit or GlycoStressKit,
894 provided by the manufacturer). Prior to measurement, calibration was started using calibration
895 plates, measuring O2 and pH LED Value/emission/Initial reference Delta for each well. After
896 calibration cartridges were kept within the machine and measurement of adipocyte-containing
897 microplates commenced. Measurement parameters were mix 3 min, wait 0 min, measure 3 min

898 with each reagent's effect assessed within three (MitoStressKit) or four consecutive measurement
899 cycles (GlycoStressKit) with a total duration of 18 min or 24 min per reagent injection. All
900 measurements started with measuring basal values, followed by injection of Oligomycin, FCCP
901 and Rotenone plus Antimycin A (MitoStressKit) or Glucose, Oligomycin and 2-Deoxy-Glucose,
902 GlycoStressKit). (1) For MitoStressKit, corresponding media were prepared before the experiment
903 and consisted of Basal Seahorse Medium supplemented with 25 mM Glucose, 1 mM Glutamine, 2
904 mM Sodium Pyruvate, set to pH = 7.4 and filtered sterile. Per Plate ca. 25 ml of MitoStress Medium
905 were needed and Seahorse cell plates were changed to 180 µl MitoStress medium 1 h prior to
906 calibration in a non-CO2 incubator at 37° C. The calibration plate possessed a cartridge having 4
907 pockets per well. Before the measurement pocket A was filled with 20 µl 10 µM Oligomycin,
908 pocket B with 22 µl 10 µM FCCP and pocket C with 25 µl 5 µM Antimycin A and Rotenone. (2)
909 For GlycoStressKit, the cell plate was washed with 1xPBS, and media changed to filtered 180 µl
910 GlycoStressKit medium. GlycoStressKit medium consisted of Basal Seahorse Medium
911 supplemented with 1 mM Glutamine and 2 mM Sodium Pyruvate, set to pH = 7.4 and stored for 1
912 h in a non-CO2 incubator at 37° C. The calibration plate possessed a cartridge having 4 pockets per
913 well. Shortly before the measurement pocket A was filled with 20 µl 10 mM Glucose, pocket B
914 with 22 µl 10 µM Oligomycin and pocket C with 25 µl 50 mM 2-Deoxy-Glucose.
915
916 *Intraperitoneal glucose tolerance test (GTT) and insulin tolerance test (ITT):*
917 GTT was carried out at 12am after a 6 h fast starting in the morning. After determining basal blood
918 glucose levels (0min), animals received an intraperitoneal bolus of 2 g glucose per kilogram of
919 body weight (20 % glucose, Delta select). Blood glucose levels were determined 15, 30, 60 and
920 120 min after injection using an automatic glucose monitor (Contour, Bayer Diabetes Care). ITT
921 was carried out in random-fed mice at 9-10am in the morning in fresh cages with bedding, free
922 access to drinking water but no food. After determining basal blood glucose levels (0min), each
923 animal received 0.75 U/kg of body weight of insulin (Actrapid; Novo Nordisk). Blood glucose
924 levels were recorded after 15, 30, 60 and 120 min. Those animals that showed no increase/decrease
925 of blood glucose levels after i.p. injection of glucose or insulin, assuming injection outside of the
926 peritoneal cavity as required for the assay, were excluded from analysis.
927
928 *Indirect calorimetry (PhenoMaster):*
929 Indirect calorimetry (PhenoMaster, TSE Systems GmbH, Bad Homburg, Germany) was used to
930 evaluate energy expenditure (EE), locomotor activity (LMA), respiratory exchange ratios (RER) as
931 well as food and water intake (1) in the animal facility of Max Planck Institute for Metabolism
932 Research or (2) the Biomedical Laboratories (University Hospital Odense, OUH). Mice were

933 allowed to acclimatize to single housing conditions in metabolic cages for two to four days. Food
934 and water were provided *ad libitum* during acclimatization and throughout all experimental
935 measurements. All parameters of indirect calorimetry were measured for a period of 1-10 days
936 depending on the duration of cold exposure. Oxygen consumption and carbon dioxide production
937 were measured in units of volume every 10 min for indicated amounts of days (including
938 measurements for both cold and warm ambient temperatures) to determine the respiratory quotient
939 (RQ = VCO2/VO2 2/VO2))) × 4.1868). LMA was measured by a multidimensional infrared light
940 beam system. Integrated scales assessed water and food intake at 2 min intervals and automatically
941 calculated cumulative water and food intake. During measurements in the PhenoMaster System,
942 mice were initially kept at a constant temperature of 23 °C for 72 h, followed by 4 °C for 1-6 days
943 depending on the experimental setup.
944
945 *mRNA isolation and quantitative RT-PCR (qPCR) analysis:*
946 mRNA isolation from primary adipocytes and adipose tissues were lysed within a monophasic
947 solution of phenol and guanidine isothiocyanate reagent (TRI Reagent®, Sigma-Aldrich #T9424)
948 and eluted with RNAse/DNAse free water following silica-based RNA spin column enrichment.
949 RNA concentrations measured by spectrophotometer and 500 ng RNA used for reverse
950 transcription (High-Capacity cDNA Reverse Transcription Kit, Thermo Fisher #4368813).
951 Abundance of *Adcy3-at*, *Adcy3-fl*, *Adipoq*, *Cidea*, *Dio2*, *Elovl3*, *Emr1*, *Fabp4*, *Lsgals3*, *Pparg*
952 isoform 2 (*Pparg2*), *Ppargc1a-at*, *Ppargc1a-fl*, *Prdm16* and *Ucp1* were quantified using SYBR
953 Green based quantification method (FastStart Universal SYBR Green Mastermix, Roche® Life
954 Science #4913914001) and mRNA abundance was calculated using relative quantification methods
955 ($2^{-\Delta\Delta CT}$). Transcript levels of mRNAs were normalized to hypoxanthine phosphoribosyltransferase
956 1 (*Hprt1*) or general transcription factor IIB (*Gtf2b*) expressions. Primer sequences for SYBR
957 Green based quantification are provided in Supplementary Table 4.
958
959 *Protein isolation:*
960 To isolate total protein from 1°BA and 1°iWA, 100-250 µl RIPA buffer were added to frozen cells
961 in cell culture plates. Using a cell scraper, the adipocytes were detached and transferred into 1.5 ml
962 reaction tubes. In case of adipose tissue, Precellys® zirconium oxide beads and 500-1000 µl RIPA
963 buffer was used to disrupt and homogenize adipose tissue using a FastPrep-24TM 5G Homogenizer
964 (mouse muscle program: 3x 90 sec). To disrupt the cell membrane of the tissue and primary cells,
965 tubes were snap frozen in liquid nitrogen and thawed on ice three times. The samples were
966 centrifuged for 10 min at 12000 x g and at 4 °C. The supernatant was transferred to a new reaction
967 tube and samples were stored at -80 °C. Quick StartTM Bradford Protein Assay Kit and Pierce

968 BCA Protein Assay Kit were used for the quantification of protein concentrations according to the
969 instructions of the kits. A FilterMaxTM F5 microplate reader was used to measure protein
970 concentrations at 595 nM.
971
972 *SDS-PAGE and Western Blot analysis:*
973 Protein samples were diluted in 4X Laemmli Buffer (Bio-Rad Laboratories) containing 5 % ß-
974 Mercaptoethanol and were boiled at 96 °C for 6 min (unless when probing for ADCY3). Protein
975 lysates were separated based on their molecular weight by sodium dodecyl sulfate-polyacrylamide
976 gel electrophoresis (SDS-PAGE). Samples and PageRulerTM Prestained Protein Ladder
977 (ThermoScientific) were loaded onto Mini-PROTEAN® precast gradient (4-20 %) polyacrylamide
978 gels (Bio-Rad Laboratories) and proteins were separated in an electric field of 90-120 V for varying
979 time spans in SDS Running Buffer (25 mM Tris-base, 0.192 M Glycine, 0.1 % SDS).
980
981 SDS-PAGE separated proteins were transferred to methanol-activated PVDF membrane by wet
982 transfer. Wet transfer was performed in a blotting chamber with ice-cold transfer buffer (48 mM
983 Tris-base, 39 mM glycine, 0.037 % SDS and 20 % methanol) for 2-3 h at 120 mA per membrane.
984 After protein transfer membranes were incubated in Ponceau solution (Sigma-Aldrich) to confirm
985 even transfer. Afterwards, membranes were rinsed once in TBS-T (500 mM Tris base, 1.5 M NaCl,
986 1 % Tween-20, pH=8) and incubated for 1 h in a Western Blocking Reagent solution (Sigma-
987 Aldrich). Membranes were incubated overnight at 4 °C with 20 ml of the respective primary
988 antibody solution. Primary antibodies were anti-HSC70 (sc-7298, Santa Cruz Biotechnology,
989 dilution 1:10,000), anti-UCP1 (#14670, Cell Signaling Technology, dilution 1:1000), anti-ADCY3
990 (#Ab14778, Abcam, dilution 1:500, and anti-phospho-PKA Substrate (#9624, Cell Signaling
991 Technology, 1:1000). Membranes were washed three times for 10 min with TBS-T and incubated
992 for 1 h at room temperature with 10 mL of the respective horseradish peroxidase (HRP)- coupled
993 secondary antibody. Wash steps were repeated, and 1 mL of chemiluminescent substrate
994 (#1705061, Biorad) was applied on the membrane and visualized by Amersham Imager 680.
995
996 For CHO cells, 4x sample buffer (200 mM TRIS/HCl pH 6.8, 8 % (w/v) SDS, 4 % (v/v) β-
997 Mercaptoethanol, 50 % (v/v) glycerin, 0.04 % (w/v) bromphenolblue) was added to the samples at a
998 final concentration of 1x, directly loaded on an 8.75 % SDS-PAGE gel, and separated by molecular
999 weight. Subsequently, proteins were transferred onto a methanol activated PVDF membrane by semi-
1000 dry transfer. The membrane was blocked using PBS Intercept blocking buffer (LI-COR) for 30 min at
1001 room temperature. The membrane was then incubated with the primary antibody solution overnight at
1002 4°C. The following primary antibodies were used: anti-FLAG (1:2000, F1804, Sigma-Aldrich) and anti-

1003 HA (1:1000, Roche, clone 3F10). Following primary antibody incubation, the membrane was washed 3
1004 times with PBS-T for 10 min at room temperature. The membrane was then incubated with the
1005 respective IRDye secondary antibodies (1:20000, LICOR) for 1 h at room temperature. After washing
1006 the membrane 3 times with PBS-T and once with PBS, protein bands were imaged using a LI-COR
1007 imaging system. Protein bands were quantified using ImageJ.
1008
1009 *Co-immunoprecipitation:*
1010 2.1 x10^6 CHO K1 cells stably expressing ADCY3-FL-HA were seeded on 10 cm cell culture dishes
1011 (Greiner). The following day, the cells were either transfected with pc3.1-ADCY3-AT-FLAG or
1012 pc3.1Zeo-mCherry using polyethylenimine (Sigma-Aldrich). To increase expression of the transfected
1013 constructs, 5 h after the transfection sodium butyrate was added to the cells to a final concentration of 5
1014 µM. 24 h later, cells were washed with 10 mL PBS and scraped in 1 mL PBS. The cell solution was then
1015 transferred into a precooled tube and centrifuged at 500 x g for 5 min at 4°C. The supernatant was
1016 aspirated, and the cell pellet resuspended in 300 µL lysis buffer (20 mM TRIS/HCl pH 8, 137 mM NaCl,
1017 2 mM EDTA, 1% NP-40, 1:500 mammalian protease inhibitor cocktail (Sigma Aldrich)). Following 60
1018 min incubation on ice, the samples were centrifuged at 10000 x g for 10 min at 4°C. The supernatant
1019 was transferred into a new tube and the protein concentration was determined using the Pierce BCA
1020 Protein Assay Kit (Thermo Scientific). Protein concentration was adjusted to 0.5 µg/µL using lysis
1021 buffer and 45 µL were stored at -80°C ("input"). To reduce the amount of unspecific binding, the lysate
1022 was incubated with uncoupled NHS-activated magnetic beads (Thermo Fisher). 40 µL NHS-activated
1023 beads were equilibrated in 400 µL equilibration buffer (10 mM TRIS/HCl pH 7.4, 150 mM NaCl) and
1024 separated from the supernatant using a magnet. The beads were resuspended in 500 µL of the 0.5 µg/µL
1025 lysate and incubated for 1 h at 4°C end over end. Beads and lysate were then magnetically separated,
1026 and 45 µL of the supernatant were stored at -80°C ('non-bound 1'). Magnetic anti-FLAG-M2 beads
1027 (Sigma-Aldrich) were equilibrated in 400 µL equilibration buffer (10 mM Tris/HCl pH=7.4, 150 mM
1028 NaCl), resuspended in the supernatant, and incubated end-over-end overnight at 4°C. The next day,
1029 beads and supernatant were magnetically separated, 45 µL of the supernatant were stored at -80°C ('non-
1030 bound 2'), and the rest of supernatants were discarded. The beads were washed 4 times with 375 µL
1031 wash buffer (20 mM TRIS/HCl pH8, 137 mM NaCl, 2 mM EDTA, 0.2 % NP-40, 1.500 mammalian
1032 protease inhibitor cocktail). 45 µL of wash fractions 1 and 4 were saved for Western blot analysis.
1033 Proteins bound to the beads were eluted by incubating the beads in 75 µL elution buffer (0.1 M glycine
1034 pH 3.0) for 3 min at room temperature. Subsequently, 20 µL 1 M TRIS/HCl pH 8 were added for
1035 neutralization. 45 µL of the neutralized elution fraction were analyzed by western blot analysis.
1036
1037 *Biotinylation assay:*

1038 The biotinylation assay was performed using the Pierce Cell Surface Biotinylation and Isolation kit
1039 (A44390, Thermo Scientific). Cells were treated with the biotinylation reagent Sulfo-NHS-SS-
1040 Biotin according to the manufacturer's protocol, harvested, and lysed. The lysate was transferred
1041 to a column containing a NeutrAvidin-agarose-resin and incubated end-over-end overnight. The
1042 column was centrifuged and the flow-through (sample F) was collected. The column was washed
1043 three times (samples W1, W2, W3) with 500 µL wash buffer and the labeled protein was eluted
1044 (sample E) using 200 µL 4x SDS sample buffer containing 50 mM dithiothreitol (DTT). After
1045 elution, beads of the agarose matrix were scraped off the column, boiled in 100 µL 4x SDS probe
1046 buffer and centrifuged. For each fraction, 40 µL were loaded.
1047
1048 *Membrane sheets and immunofluorescent labeling:*
1049 CHO cells were seeded on poly-L-lysine (PLL, 0.1 mg/ml, Sigma Aldrich, #P1399-100MG)-coated 13
1050 mm glass coverslips (VWR) coated glass coverslips in a 4-well dish (VWR) and cultured for 24 h.
1051 Before sonification, cells were washed with PBS and sonicated in 500 µl sonification buffer (120 mM
1052 glutamate, 20 mM potassium acetate, 10 mM HEPES, 10 mM EGTA, pH 7.2 using the VibraCell
1053 Sonifier (0.1 s pulse, distance to cover slip: 3 mm, amplitude: 1-20 %). Cells were fixed with 4 %
1054 paraformaldehyde (Alfa Aesar, ThermoFisher Scientific, #43368) for 10 min at room temperature. After
1055 washing thrice with PBS, cells were blocked with CT (0.5% Triton X-100 (Sigma Aldrich, #X100) and
1056 5% ChemiBLOCKER (Merck Millipore, #2170) in 0.1 M NaP, pH 7.0) for 30 min at room temperature.
1057 Primary and secondary antibodies were diluted in CT and incubated for 60 min each at room
1058 temperature, respectively. Coverslips were mounted with one drop of Aqua-Poly/Mount (Tebu-Bio,
1059 #07918606-20). The following primary antibodies were used: anti-calnexin (rb, 1:200, Sigma Aldrich,
1060 #C4731), anti-HA (rt, 1:1000, Roche, clone 3F10), anti-CNG channel (ms, 1:100, clone 3B10) (Pichlo
1061 et al, JCB 2014). As a DNA counterstain, cells were labeled with DAPI together with the secondary
1062 antibody (4',6-Diamidino-2-Phenylindole, Dihydrochloride, 1:10.000, Thermo Fisher Scientific,
1063 #D1306). The following secondary antibodies were used: goat-anti-rabbit-Alexa647 (1:500, Thermo
1064 Fisher Scientific, #A21245), goat-anti-mouse-Alexa594 (1:500, Thermo Fisher Scientific, #A21125),
1065 goat-anti-rat-Alexa488 (1:500, Thermo Fisher Scientific, #A11006).
1066
1067 *AlphaFold modeling of Adcy3 structures:*
1068 Folding prediction of ADCY3-FL and ADCY3-AT protein monomers and dimers were carried out
1069 with LocalColabFold based on AlphaFold2 using standard parameters [54, 87]. ATP was docked to
1070 ADCY3 models by aligning catalytic domains with B chain of x-ray crystal structure PDB ID 3C16
1071 (Catalytic Domain of Mammalian Adenylyl Cyclase). Computation of the models was performed
1072 on the UCloud interactive HPC system, which is managed by the eScience Center at the University

1073 of Southern Denmark. Molecular graphics performed with UCSF ChimeraX[88]. Alignment of
1074 structures was performed using '*mmaker*' function in ChimeraX.
1075
1076 *PamGene serine-threonine kinase (STK) kinome arrays:*
1077 Frozen brown adipose tissue was homogenized in 150 µL cold M-Per (Thermo Fisher) containing 1:50
1078 HALT Protease and Phosphatase Inhibitor Cocktail (EDTA-free, 100x, Thermo Fisher) using a small,
1079 precooled pistil. Following 10 min incubation on ice, samples were centrifuged at 10000 x g for 5 min
1080 at 4°C. The liquid phase was carefully transferred into a new precooled tube, and this process was
1081 repeated at least twice (or until no lipid phase was left). Subsequently, the cleared lysates were aliquoted
1082 in 15 µL aliquots, frozen in liquid nitrogen, and stored at -80°C. Not more than 4 samples were handled
1083 simultaneously to avoid prolonged handling times. After the protein concentration was determined using
1084 Pierce BCA Protein Assay Kit (Thermo Scientific), 10 µg of protein was used as input and the STK
1085 assay was performed according to the standard protocol provided by PamGene. Kinome trees have been
1086 generated using the following software: http://phanstiel-lab.med.unc.edu/CORAL/
1087
1088 *Catch point cAMP assay (ELISA):*
1089 Brown adipose tissue cAMP levels were measured using the CatchPoint cAMP Fluorescent Assay Kit
1090 (Molecular Devices). A small piece of frozen BAT (2 – 5 mg) was transferred into a BeadBug tube
1091 (Sigma Aldrich) containing 1.0 mm zirconium beads (Merck) and 300 µL cold catchpoint lysis buffer.
1092 The tissue was disrupted using a BeadBug microtube homogenizer (Sigma Aldrich) at 400 rpm for 30
1093 s. Subsequently, samples were placed on ice for 1 min and homogenization was repeated twice.
1094 Following 15 min incubation at 4°C, each sample was sonicated 3 times for 1 min with 1 min incubation
1095 on ice in between each cycle. To clear the lysate from debris and insoluble lipids, samples were
1096 centrifuged at 10000 x g for 10 min at 4°C. The liquid fraction of the lysate was then transferred into a
1097 new tube and the process was repeated twice. The protein concentration of the cleared lysate was
1098 determined using the Pierce BCA Protein Assay Kit (Thermo Scientific). The CatchPoint cAMP ELISA
1099 was then performed according to the manual using 0.8 µg protein as input. Colorimetric measurement
1100 was performed after 30 min final incubation using a FLUOstar Omega (BMG Labtech).
1101
1102 *Human primary brown and white adipocytes and study characteristics:*
1103 Primary human BA were isolated as described [76] and cultured in 60mm culture dishes containing
1104 DMEM/F12, 10% FBS, 1% Penicillin/Streptomycin (all from Invitrogen) and 1nM acidic FGF-1
1105 (ImmunoTools). Cells were incubated at 37°C with 5% CO2. Adipocytes were induced two days
1106 after full confluence with DMEM/F12 containing 1% Penicillin/Streptomycin, 0.1 mM
1107 dexamethasone (Sigma-Aldrich), 100 nM insulin, 200 nM rosiglitazone (Sigma-Aldrich), 540 mM

1108 isobutylmethylxanthine (Sigma-Aldrich), 2 nM T3 (Sigma-Aldrich) and 10 mg/mL transferrin
1109 (Sigma-Aldrich). After three days of differentiation, isobutylmethylxanthine was removed from the
1110 cell culture media. The cell cultures were left to differentiate for an additional nine days. Cells were
1111 treated with and without 1 µM NE for 16h. Total RNA was isolated using Trizol (Invitrogen).
1112 Reverse transcription was performed using ProtoScript II (NEB, Bonn). qPCR reactions were
1113 assembled with Luna Master Mix (NEB) and qPCR was performed using a HT7900 (Applied
1114 Biosystems, Bonn). Expression levels were calculated as delta Ct values relative to house-keeping
1115 gene *hTBP* serving as housekeeping control. Primer details are provided in Supplementary Table
1116 S4. The generation of human brown adipocytes was approved by vote 076/18 of the ethical
1117 committee of the University of Bonn.
1118
1119 *Comparative sequence conservation analyses of Adcy3-at and Ppargc1a-at genomic sequences:*
1120 Analyses of alternative transcription (AT) start sites sequence conservation were conducted by first
1121 acquiring genomic contigs spanning either *Ppargc1a* or *Adcy3* via NCBI BLASTs using mouse or
1122 human transcript variants (accession numbers: NM_001377131.1; NM_138305.3; NR_132764.1)
1123 as query against whole genome shotgun contigs from representative species. Accession numbers
1124 of acquired contigs are listed in Supplementary Table S2. Contigs were imported into Geneious
1125 software version 9.1.8 (Dotmatics), and conserved exons were annotated using the 'transfer
1126 annotations' function. Alternative start sites from the mouse or human were then used to search for
1127 homologous sequences among contigs of various species using either the 'transfer annotations'
1128 function or EMBOSS 6.5.7 dotmatcher dot plots. MUSCLE alignments of conserved putative AT
1129 regions were assembled in Geneious and pairwise percent nucleotide identities were calculated
1130 relative to AT sites of either the mouse or human. These conservation levels were then mapped to
1131 the respective phylogenetic trees using the colour gradient function on the Interactive Tree of Life
1132 webserver[89]. The phylogenetic relationships and branch lengths illustrating the conservation of
1133 *Ppargc1a-at* were based on [77], while phylogenetic relationships and branch lengths for *Adcy3-at*
1134 conservation analyses were based on [90] for primates and [91] for rodents.
1135
1136 *Data availability:*
1137 NGS datasets are currently being uploaded to Gene Expression Omnibus (GEO) and are provided
1138 upon reviewer's request.
1139
1140 *Public datasets:*
1141 H3K4me3 ChIP-seq from BAT of chow diet and HFD fed, male C57BL/6N mice housed at 22°C
1142 or exposed to 5°C for 24 h were downloaded from GEO (GSE20065). snRNA-seq data from

1143 *Adipoq*-tdTomato-positive adipocyte nuclei were downloaded from Array Express (E-MTAB-
1144 8562).

References:

1. Kusminski, C.M., Bickel, P.E. & Scherer, P.E. Targeting adipose tissue in the treatment of obesity-associated diabetes. *Nature reviews. Drug discovery* **15**, 639-660 (2016).
2. Cannon, B. & Nedergaard, J. Brown adipose tissue: function and physiological significance. *Physiol Rev* **84**, 277-359 (2004).
3. van Marken Lichtenbelt, W.D. *et al.* Cold-activated brown adipose tissue in healthy men. *The New England journal of medicine* **360**, 1500-1508 (2009).
4. Cypess, A.M. *et al.* Identification and importance of brown adipose tissue in adult humans. *The New England journal of medicine* **360**, 1509-1517 (2009).
5. Virtanen, K.A. *et al.* Functional brown adipose tissue in healthy adults. *The New England journal of medicine* **360**, 1518-1525 (2009).
6. Yoneshiro, T. *et al.* Recruited brown adipose tissue as an antiobesity agent in humans. *The Journal of clinical investigation* **123**, 3404-3408 (2013).
7. Cypess, A.M. *et al.* Activation of human brown adipose tissue by a beta3-adrenergic receptor agonist. *Cell metabolism* **21**, 33-38 (2015).
8. Mueller, E. Browning and Graying: Novel Transcriptional Regulators of Brown and Beige Fat Tissues and Aging. *Frontiers in endocrinology* **7**, 19 (2016).
9. Marti-Solano, M. *et al.* Combinatorial expression of GPCR isoforms affects signalling and drug responses. *Nature* **587**, 650-656 (2020).
10. Ceddia, R.P. & Collins, S. A compendium of G-protein-coupled receptors and cyclic nucleotide regulation of adipose tissue metabolism and energy expenditure. *Clinical science (London, England : 1979)* **134**, 473-512 (2020).
11. Kajimura, S., Spiegelman, B.M. & Seale, P. Brown and Beige Fat: Physiological Roles beyond Heat Generation. *Cell metabolism* **22**, 546-559 (2015).
12. Blondin, D.P. *et al.* Human Brown Adipocyte Thermogenesis Is Driven by β2-AR Stimulation. *Cell metabolism* **32**, 287-300.e287 (2020).
13. Khannpnavar, B., Mehta, V., Qi, C. & Korkhov, V. Structure and function of adenylyl cyclases, key enzymes in cellular signaling. *Curr Opin Struct Biol* **63**, 34-41 (2020).
14. Reverte-Salisa, L., Sanyal, A. & Pfeifer, A. Role of cAMP and cGMP Signaling in Brown Fat. *Handb Exp Pharmacol* **251**, 161-182 (2019).
15. Wu, L., Shen, C., Seed Ahmed, M., Ostenson, C.G. & Gu, H.F. Adenylate cyclase 3: a new target for anti-obesity drug development. *Obes Rev* **17**, 907-914 (2016).
16. Stergiakouli, E. *et al.* Genome-wide association study of height-adjusted BMI in childhood identifies functional variant in ADCY3. *Obesity* **22**, 2252-2259 (2014).
17. Saeed, S. *et al.* Loss-of-function mutations in ADCY3 cause monogenic severe obesity. *Nature genetics* **50**, 175-179 (2018).
18. Grarup, N. *et al.* Loss-of-function variants in ADCY3 increase risk of obesity and type 2 diabetes. *Nature genetics* **50**, 172-174 (2018).
19. Toumba, M. *et al.* Molecular modelling of novel ADCY3 variant predicts a molecular target for tackling obesity. *Int J Mol Med* **49** (2022).
20. Tong, T., Shen, Y., Lee, H.W., Yu, R. & Park, T. Adenylyl cyclase 3 haploinsufficiency confers susceptibility to diet-induced obesity and insulin resistance in mice. *Scientific reports* **6**, 34179 (2016).
21. Wang, Z. *et al.* Adult type 3 adenylyl cyclase-deficient mice are obese. *PloS one* **4**, e6979 (2009).
22. Wong, S.T. *et al.* Disruption of the type III adenylyl cyclase gene leads to peripheral and behavioral anosmia in transgenic mice. *Neuron* **27**, 487-497 (2000).
23. Pitman, J.L. *et al.* A gain-of-function mutation in adenylate cyclase 3 protects mice from diet-induced obesity. *PloS one* **9**, e110226 (2014).
24. Chen, X. *et al.* Ablation of Type III Adenylyl Cyclase in Mice Causes Reduced Neuronal Activity, Altered Sleep Pattern, and Depression-like Phenotypes. *Biological psychiatry* **80**, 836-848 (2016).

1198 25. Chao, Y. *et al.* Regulatory roles and mechanisms of alternative RNA splicing in adipogenesis
1199 and human metabolic health. *Cell Biosci* **11**, 66 (2021).
1200 26. Lin, J.C., Lu, Y.H., Liu, Y.R. & Lin, Y.J. RBM4a-regulated splicing cascade modulates the
1201 differentiation and metabolic activities of brown adipocytes. *Scientific reports* **6**, 20665 (2016).
1202 27. Vernia, S. *et al.* An alternative splicing program promotes adipose tissue thermogenesis. *eLife*
1203 **5** (2016).
1204 28. Ruas, J.L. *et al.* A PGC-1alpha isoform induced by resistance training regulates skeletal muscle
1205 hypertrophy. *Cell* **151**, 1319-1331 (2012).
1206 29. Jannig, P.R., Dumesic, P.A., Spiegelman, B.M. & Ruas, J.L. SnapShot: Regulation and biology
1207 of PGC-1alpha. *Cell* **185**, 1444-1444 e1441 (2022).
1208 30. Li, Y. *et al.* Comparative Transcriptome Profiling of Cold Exposure and beta3-AR Agonist
1209 CL316,243-Induced Browning of White Fat. *Front Physiol* **12**, 667698 (2021).
1210 31. Omori, K. & Kotera, J. Overview of PDEs and their regulation. *Circ Res* **100**, 309-327 (2007).
1211 32. Granneman, J.G. Expression of adenylyl cyclase subtypes in brown adipose tissue: neural
1212 regulation of type III. *Endocrinology* **136**, 2007-2012 (1995).
1213 33. Son, Y. *et al.* REEP6 knockout leads to defective beta-adrenergic signaling in adipocytes and
1214 promotes obesity-related metabolic dysfunction. *Metabolism* **130**, 155159 (2022).
1215 34. Sun, W. *et al.* snRNA-seq reveals a subpopulation of adipocytes that regulates thermogenesis.
1216 *Nature* **587**, 98-102 (2020).
1217 35. Perdikari, A. *et al.* BATLAS: Deconvoluting Brown Adipose Tissue. *Cell reports* **25**, 784-797
1218 e784 (2018).
1219 36. Eguchi, J. *et al.* Transcriptional control of adipose lipid handling by IRF4. *Cell metabolism* **13**,
1220 249-259 (2011).
1221 37. Hamann, A., Flier, J.S. & Lowell, B.B. Decreased brown fat markedly enhances susceptibility
1222 to diet-induced obesity, diabetes, and hyperlipidemia. *Endocrinology* **137**, 21-29 (1996).
1223 38. Li, F. *et al.* Epigenetic interaction between UTX and DNMT1 regulates diet-induced myogenic
1224 remodeling in brown fat. *Nature communications* **12**, 6838 (2021).
1225 39. Schmidt, E. *et al.* LincRNA H19 protects from dietary obesity by constraining expression of
1226 monoallelic genes in brown fat. *Nature communications* **9**, 3622 (2018).
1227 40. Oliverio, M. *et al.* Dicer1-miR-328-Bace1 signalling controls brown adipose tissue
1228 differentiation and function. *Nature cell biology* **18**, 328-336 (2016).
1229 41. Feldmann, H.M., Golozoubova, V., Cannon, B. & Nedergaard, J. UCP1 ablation induces obesity
1230 and abolishes diet-induced thermogenesis in mice exempt from thermal stress by living at
1231 thermoneutrality. *Cell metabolism* **9**, 203-209 (2009).
1232 42. Cao, W. *et al.* p38 mitogen-activated protein kinase is the central regulator of cyclic AMP-
1233 dependent transcription of the brown fat uncoupling protein 1 gene. *Molecular and cellular*
1234 *biology* **24**, 3057-3067 (2004).
1235 43. Lindquist, J.M. & Rehnmark, S. Ambient temperature regulation of apoptosis in brown adipose
1236 tissue. Erk1/2 promotes norepinephrine-dependent cell survival. *The Journal of biological*
1237 *chemistry* **273**, 30147-30156 (1998).
1238 44. Hattori, K. *et al.* beta-adrenergic receptor signaling evokes the PKA-ASK axis in mature brown
1239 adipocytes. *PloS one* **15**, e0232645 (2020).
1240 45. Ji, H. *et al.* CDK7 Mediates the Beta-Adrenergic Signaling in Thermogenic Brown and White
1241 Adipose Tissues. *iScience* **23**, 101163 (2020).
1242 46. Roh, H.C. *et al.* Warming Induces Significant Reprogramming of Beige, but Not Brown,
1243 Adipocyte Cellular Identity. *Cell metabolism* **27**, 1121-1137 e1125 (2018).
1244 47. Pan, D. *et al.* Jmjd3-Mediated H3K27me3 Dynamics Orchestrate Brown Fat Development and
1245 Regulate White Fat Plasticity. *Developmental cell* **35**, 568-583 (2015).
1246 48. Brunmeir, R. *et al.* Comparative Transcriptomic and Epigenomic Analyses Reveal New
1247 Regulators of Murine Brown Adipogenesis. *PLoS genetics* **12**, e1006474 (2016).
1248 49. Engelhard, C.A. *et al.* Comprehensive Transcriptional Profiling and Mouse Phenotyping
1249 Reveals Dispensable Role for Adipose Tissue Selective Long Noncoding RNA Gm15551.
1250 *Noncoding RNA* **8** (2022).

1251 50. Darcy, J. & Tseng, Y.H. ComBATing aging-does increased brown adipose tissue activity confer
1252 longevity? *Geroscience* **41**, 285-296 (2019).
1253 51. Crossthwaite, A.J., Ciruela, A., Rayner, T.F. & Cooper, D.M. A direct interaction between the
1254 N terminus of adenylyl cyclase AC8 and the catalytic subunit of protein phosphatase 2A. *Mol*
1255 *Pharmacol* **69**, 608-617 (2006).
1256 52. Ding, Q., Gros, R., Chorazyczewski, J., Ferguson, S.S. & Feldman, R.D. Isoform-specific
1257 regulation of adenylyl cyclase function by disruption of membrane trafficking. *Mol Pharmacol*
1258 **67**, 564-571 (2005).
1259 53. Lang, T. Imaging SNAREs at work in 'unroofed' cells--approaches that may be of general
1260 interest for functional studies on membrane proteins. *Biochem Soc Trans* **31**, 861-864 (2003).
1261 54. Jumper, J. *et al.* Highly accurate protein structure prediction with AlphaFold. *Nature* **596**, 583-
1262 589 (2021).
1263 55. Lin, J., Handschin, C. & Spiegelman, B.M. Metabolic control through the PGC-1 family of
1264 transcription coactivators. *Cell metabolism* **1**, 361-370 (2005).
1265 56. Huang, P.I. *et al.* PGC-1alpha mediates differentiation of mesenchymal stem cells to brown
1266 adipose cells. *J Atheroscler Thromb* **18**, 966-980 (2011).
1267 57. Liu, Z. *et al.* Nterminal truncated peroxisome proliferatoractivated receptorgamma
1268 coactivator1alpha alleviates phenylephrineinduced mitochondrial dysfunction and decreases
1269 lipid droplet accumulation in neonatal rat cardiomyocytes. *Mol Med Rep* **18**, 2142-2152 (2018).
1270 58. Zhang, J.W., Klemm, D.J., Vinson, C. & Lane, M.D. Role of CREB in transcriptional regulation
1271 of CCAAT/enhancer-binding protein beta gene during adipogenesis. *The Journal of biological*
1272 *chemistry* **279**, 4471-4478 (2004).
1273 59. Zhang, Y. *et al.* Alternative mRNA splicing produces a novel biologically active short isoform
1274 of PGC-1alpha. *The Journal of biological chemistry* **284**, 32813-32826 (2009).
1275 60. Kim, J. *et al.* NT-PGC-1alpha deficiency attenuates high-fat diet-induced obesity by modulating
1276 food intake, fecal fat excretion and intestinal fat absorption. *Scientific reports* **11**, 1323 (2021).
1277 61. Martinez-Redondo, V., Pettersson, A.T. & Ruas, J.L. The hitchhiker's guide to PGC-1alpha
1278 isoform structure and biological functions. *Diabetologia* **58**, 1969-1977 (2015).
1279 62. Finck, B.N. & Kelly, D.P. PGC-1 coactivators: inducible regulators of energy metabolism in
1280 health and disease. *The Journal of clinical investigation* **116**, 615-622 (2006).
1281 63. Durham, A.L., Speer, M.Y., Scatena, M., Giachelli, C.M. & Shanahan, C.M. Role of smooth
1282 muscle cells in vascular calcification: implications in atherosclerosis and arterial stiffness.
1283 *Cardiovasc Res* **114**, 590-600 (2018).
1284 64. Clement, N., Glorian, M., Raymondjean, M., Andreani, M. & Limon, I. PGE2 amplifies the
1285 effects of IL-1beta on vascular smooth muscle cell de-differentiation: a consequence of the
1286 versatility of PGE2 receptors 3 due to the emerging expression of adenylyl cyclase 8. *J Cell*
1287 *Physiol* **208**, 495-505 (2006).
1288 65. Keuylian, Z. *et al.* The Notch pathway attenuates interleukin 1beta (IL1beta)-mediated
1289 induction of adenylyl cyclase 8 (AC8) expression during vascular smooth muscle cell (VSMC)
1290 trans-differentiation. *The Journal of biological chemistry* **287**, 24978-24989 (2012).
1291 66. Hewer, R.C., Sala-Newby, G.B., Wu, Y.J., Newby, A.C. & Bond, M. PKA and Epac
1292 synergistically inhibit smooth muscle cell proliferation. *J Mol Cell Cardiol* **50**, 87-98 (2011).
1293 67. McKean, J.S. *et al.* The cAMP-producing agonist beraprost inhibits human vascular smooth
1294 muscle cell migration via exchange protein directly activated by cAMP. *Cardiovasc Res* **107**,
1295 546-555 (2015).
1296 68. Vallin, B. *et al.* Novel short isoforms of adenylyl cyclase as negative regulators of cAMP
1297 production. *Biochim Biophys Acta Mol Cell Res* **1865**, 1326-1340 (2018).
1298 69. Hu, B., Nakata, H., Gu, C., De Beer, T. & Cooper, D.M. A critical interplay between Ca2+
1299 inhibition and activation by Mg2+ of AC5 revealed by mutants and chimeric constructs. *The*
1300 *Journal of biological chemistry* **277**, 33139-33147 (2002).
1301 70. Montminy, M. Transcriptional regulation by cyclic AMP. *Annual review of biochemistry* **66**,
1302 807-822 (1997).

71. Li, Y. *et al.* Clenbuterol upregulates histone demethylase JHDM2a via the beta2-adrenoceptor/cAMP/PKA/p-CREB signaling pathway. *Cellular signalling* **24**, 2297-2306 (2012).
72. Muglia, L.M. *et al.* The 5'-flanking region of the mouse adenylyl cyclase type VIII gene imparts tissue-specific expression in transgenic mice. *The Journal of neuroscience : the official journal of the Society for Neuroscience* **19**, 2051-2058 (1999).
73. Chao, J.R. *et al.* Characterization of the mouse adenylyl cyclase type VIII gene promoter: regulation by cAMP and CREB. *Eur J Neurosci* **16**, 1284-1294 (2002).
74. Chinsomboon, J. *et al.* The transcriptional coactivator PGC-1alpha mediates exercise-induced angiogenesis in skeletal muscle. *Proceedings of the National Academy of Sciences of the United States of America* **106**, 21401-21406 (2009).
75. Tang, A.D. *et al.* Full-length transcript characterization of SF3B1 mutation in chronic lymphocytic leukemia reveals downregulation of retained introns. *Nature communications* **11**, 1438 (2020).
76. Jespersen, N.Z. *et al.* A classical brown adipose tissue mRNA signature partly overlaps with brite in the supraclavicular region of adult humans. *Cell metabolism* **17**, 798-805 (2013).
77. Meredith, R.W. *et al.* Impacts of the Cretaceous Terrestrial Revolution and KPg extinction on mammal diversification. *Science* **334**, 521-524 (2011).
78. Cong, L. *et al.* Multiplex genome engineering using CRISPR/Cas systems. *Science* **339**, 819-823 (2013).
79. Zhang, M. *et al.* Recessive cardiac phenotypes in induced pluripotent stem cell models of Jervell and Lange-Nielsen syndrome: disease mechanisms and pharmacological rescue. *Proceedings of the National Academy of Sciences of the United States of America* **111**, E5383-5392 (2014).
80. Patro, R., Duggal, G., Love, M.I., Irizarry, R.A. & Kingsford, C. Salmon provides fast and bias-aware quantification of transcript expression. *Nature methods* **14**, 417-419 (2017).
81. Soneson, C., Love, M.I. & Robinson, M.D. Differential analyses for RNA-seq: transcript-level estimates improve gene-level inferences. *F1000Res* **4**, 1521 (2015).
82. Robinson, M.D., McCarthy, D.J. & Smyth, G.K. edgeR: a Bioconductor package for differential expression analysis of digital gene expression data. *Bioinformatics* **26**, 139-140 (2010).
83. Yu, G., Wang, L.G., Han, Y. & He, Q.Y. clusterProfiler: an R package for comparing biological themes among gene clusters. *OMICS* **16**, 284-287 (2012).
84. Li, H. Minimap2: pairwise alignment for nucleotide sequences. *Bioinformatics* **34**, 3094-3100 (2018).
85. Hahne, F. & Ivanek, R. Visualizing Genomic Data Using Gviz and Bioconductor. *Methods in molecular biology* **1418**, 335-351 (2016).
86. Hao, Y. *et al.* Integrated analysis of multimodal single-cell data. *Cell* **184**, 3573-3587 e3529 (2021).
87. Mirdita, M. *et al.* ColabFold: making protein folding accessible to all. *Nature methods* **19**, 679-682 (2022).
88. Pettersen, E.F. *et al.* UCSF ChimeraX: Structure visualization for researchers, educators, and developers. *Protein Sci* **30**, 70-82 (2021).
89. Letunic, I. & Bork, P. Interactive Tree Of Life (iTOL) v5: an online tool for phylogenetic tree display and annotation. *Nucleic acids research* **49**, W293-W296 (2021).
90. Perelman, P. *et al.* A molecular phylogeny of living primates. *PLoS genetics* **7**, e1001342 (2011).
91. Swanson, M.T., Oliveros, C.H. & Esselstyn, J.A. A phylogenomic rodent tree reveals the repeated evolution of masseter architectures. *Proc Biol Sci* **286**, 20190672 (2019).

Acknowledgements:

We thank Jens Alber and Ann-Brit Marcher for indirect calorimetry (TSE Phenomaster) support.

Sequencing was carried out at the Functional Genomics and Metabolism Research Unit, University

of Southern Denmark. The authors thank Tenna P. Mortensen, Maibrith Wishoff, and Ronni Nielsen for sequencing assistance. We thank Catharina Baitzel and Anke Lietzau, Max-Planck Institute for Metabolism Research, for assistance in generating *Adcy3*Δ*AT* mice. JWK and BDL received funding from the University of Southern Denmark and the Danish Diabetes Academy, which is funded by the Novo Nordisk Foundation. JWK, AJ, and ARAAT received support from Challenge (#33444) and Bioscience and Basic Biomedicine Programs of the NNF (#28416). HT is supported by a postdoctoral fellowship form the DDA. SK was supported by a German Academic Exchange Service (DAAD) PhD scholarship (A/12/97620). We to thank the Microscopy Core Facility of the Medical Faculty at the University of Bonn for providing help, services, and devices funded by the Deutsche Forschungsgemeinschaft (DFG, German Research Foundation) – project numbers 169331223, 388159768. Research in the Wachten lab was supported by grants from the DFG – SFB 1454 – project number 432325352, TRR83 – 112927078, TRR333/1 – 450149205, under Germany's Excellence Strategy – EXC2151 – 390873048, SPP1926, SPP1726, FOR2743 as well as intramural funding from the University of Bonn. AP and TG are funded by the DFG (Deutsche Forschungsgemeinschaft) 450149205-TRR333/1 (AP: P10; TG: P11).

Authors contributions:

SK, HT, AJ, PL, BDL, ARAAT, NS, IG, NH, ES, RR, SG, LMV, TG, SN, MPJ, NZJ performed the experiments. SK, HT, AJ, PL, IG, AP, TG, MJ, MG, BDL, CAE, MG, RR, PK contributed discussions and performed training. SK, HT, AJ, PL, BDL, NH, PF, ARA, SN, CMS, TJS, FTW, AP, MJ, DW and JWK conceived the experiments. DW, HT and JWK wrote the manuscript.

Competing financial interests:

The authors declare no conflicting financial interest.

Materials & Correspondence:

Requests should be addressed to Jan-Wilhelm Kornfeld (janwilhelmkornfeld@bmb.sdu.dk) or Dagmar Wachten (dwachten@uni-bonn.de).

1382 ***Supplementary information:***

1383

1384 **Supplementary Figure S1: Transcriptional regulation of cAMP biosynthesis in adipose tissue**
1385 **after cold exposure.** (**a-c**) Principal component analysis (PCA) of transcriptomic changes in (**a**)
1386 BAT, (**b**) iWAT and (**c**) eWAT after 24 h (**a,c**) or 72 h (**b**) of 5° cold exposure. Dots represent
1387 individual, chow diet fed male C57BL/6N animals with n=3-5 animals per temperature condition
1388 (**d-f**). mRNA expression of phosphodiesterases (PDEs) mRNA abundance in BAT (**d**), iWAT (**e**)
1389 and eWAT (**f**) determined by mRNA-seq and depicted in transcripts per million (TPM). (**d-f**) Bar
1390 graphs represent mean ± SD with all data points plotted. Unpaired, two-tailed, and non-parametric
1391 Mann-Whitney tests were performed to assess statistical significance.

1392

1393 **Supplementary Figure S2: ADCY3 is required for cAMP biosynthesis in BAT and required**
1394 **for cold adaptation in cold.** (**a-b**) Expression of indicated (**a**) transcriptional BAT regulator genes
1395 and (**b**) adipose depot specific genes in BAT from *LoxP* (n=4 each for 22°C and 5°C) and *Adcy3-*
1396 *AdcKO* mice (n=4 each for 22°C and 5°C) housed at 22°C or after 24 h of 5°C cold exposure as
1397 determined by mRNA-seq and depicted in transcripts per million (TPM). (**c-d**) qPCR analysis of
1398 indicated BAT mRNA markers measured in 1°BA derived from SVF of *LoxP* animals (**c**) or *LoxP*
1399 and *Adcy3-AdcKO* mice (**d**). (**c-d**) Replicates represent n=4 primary brown adipocytes, n=4 mice
1400 per adipose depot, stimulation regimen and genotype. Bar graphs represent mean ± SD with all data
1401 points plotted. To test for statistical significance, non-parametric (ranked) Kruskal–Wallis one-way
1402 analysis of variance (ANOVA) tests with Dunn's correction for multiple testing were performed.

1403

1404 **Supplementary Figure S3: ADCY3 loss in adipocytes predisposes to obesity-associated brown**
1405 **fat dysfunction.** (**a-b**) Relative (body-weight corrected) gross tissue weights from indicated
1406 adipose tissue depots and liver from *LoxP* (*n=4* for 22°C, n=8 for 5°C) and *Adcy3-AdcKO* mice
1407 (*n=4* for 22°C, n=8 for 5°C) fed (**a**) chow diet or (**b**) HFD and housed at 22°C (*left side of panels*)
1408 or exposed for 24 h to 5°C (*right side of panels*). Bar graphs represent mean ± SD with all data
1409 points plotted. Unpaired, two-tailed, and non-parametric Mann-Whitney tests were performed to
1410 assess statistical significance. (**c-d,f**) Analysis of STK activity in murine brown adipose tissue.
1411 Kinome trees depict the mean kinase statistic of differentially activated STKs in (**c**) LoxP (22°C vs
1412 5°, 24 h), (**d**) LoxP (22°C vs 5°, 6 days) and (**f**) *Adcy3-AdcKO* vs. *LoxP* (22°C). Inserts show zoom-
1413 ins of relevant areas of the kinome tree (blue box: down-regulated kinases; red box: up-regulated
1414 kinases). (**c-d,ii**) Mean kinase statistic of 15 most significantly differentially activated kinases is
1415 represented in bar graphs. (**f,iii**) Venn diagram depicting differences in differentially activated
1416 kinases of the respective comparison. Data represent mean of n=4 biological replicates for all

1417 conditions. (**e**) Protein immunoblots of BAT from chow-diet fed, male *LoxP* and *Adcy3-AdcKO*
1418 mice housed at room temperature (22°C) or for 6 days in the cold (5°C). Anti-phospho-PKA
1419 substrate antibodies were used for detection of PKA phosphorylation substrates. Anti-UCP1
1420 antibodies probed for UCP1 protein levels. anti-HSC70 antibody served as loading control.
1421
1422 **Supplementary Figure S4: Activated brown adipocytes express a truncated ADCY3**
1423 **(ADCY3-AT) transcript and protein isoform.** (**a**) Genome browser track depicting changes in
1424 mRNA expression (grey) and H3K4me3 (magenta) in BAT from chow diet-fed, male C57BL/6N
1425 mice housed at 22°C or exposed to 24 h of 5°C cold challenge. Red and blue transcripts depict
1426 *Adcy3-fl* and *Adcy3-at* transcripts, respectively, and mRNA isoform specific transcriptional start
1427 sites (TSS). (**b**) ChIP-qPCR of H3K4me3 at the TSS of *Adcy3-fl* (blue), *Adcy3-at* (red) and *Adcy3-*
1428 *fl* and *Adcy3-at* common exon 3 (grey). Replicates represent H3K4me3 immunoprecipitations
1429 perform in individual animals (n=3). Bar graphs represent mean ± SD with all data points plotted.
1430 To test for statistical significance, parametric, unpaired, two-tailed Student's t-tests were
1431 performed. *P*-values are indicated in the panel. (**c-d**) Expression of (**c**) *Adcy3-fl* (blue) and (**d**)
1432 *Adcy3-at* (red) in indicated whole tissues from chow diet fed, male C57BL/6N mice. Data points
1433 represent individual mice (n=4 BAT, n=2 iWAT, n=3 eWAT, n=3 pancreas, n=3 kidneys, n=2
1434 skeletal muscle, n=3 liver). (**e-g**) Absolute expression (ΔΔCt) of (**e**)*Adcy3-at*, (**f**) *Ucp1* and (**g**)
1435 *Adcy3-fl* in BAT-derived SVF at indicated stages of brown adipogenesis and after stimulation with
1436 1 mM db-cAMP or 10 µM CL316,243 as determined by qPCR. Replicates depict experiments
1437 performed in SVF isolated from individual mice, i.e., n=4 biological replicates. Bar graphs
1438 represent mean ± SD with all data points. (**h**,**i**) Expression of indicated mRNAs in (**h**) BAT or (**i**)
1439 iWAT of chow diet or HFD fed male C57BL/6N mice housed at 22°C or after 24 h of 5°C cold
1440 exposure as determined by qPCR. Bar graphs represent mean ± SD with all data points plotted. To
1441 test for statistical significance, non-parametric (ranked) Kruskal–Wallis one-way analysis of
1442 variance (ANOVA) tests with Dunn's correction for multiple testing were performed. *P*-values are
1443 indicated in the panel. (**j**) Expression of *Adcy3-at* in BAT of chow diet fed male C57BL/6N mice
1444 at 2.5 months or 25 months of age. Bar graphs represent mean ± SD with all data points plotted.
1445
1446 **Supplementary Figure S5: ADCY3-AT inhibits oxidative metabolism *in vitro* and *in vivo*.** (**a**)
1447 Genome browser track depicting mRNA (grey) and H3K4me3 signals in murine *Adcy3* locus from
1448 chow diet fed, male C57BL/6N mice at 22° (light grey) and 5°C (dark grey) as well as HFD-fed,
1449 male C57BL/6N mice at 22°C (light orange) and 5°C (dark orange). Location and sequence of
1450 sgRNAs used for CRISPR/Cas9 mediated 978-nt deletion *Adcy3-at* TSS are indicated. (**b**) Southern
1451 blot analysis of control (C57BL/6N wildtype, WT) and *Adcy3*Δ*AT* embryonic stem cell DNA. The

1452 asterisk depicts a heterozygous *ADCY3ΔAT*/WT ESC. (**c**) PCR from genomic DNA isolated from
1453 *Adcy3-at* proficient (WT) and *Adcy3ΔAT* embryonic stem cell DNA. (**d,h**) Blood glucose excursion
1454 during insulin tolerance tests performed in (**d**) chow diet and (**h**) HFD fed, male *LoxP* (n=7 chow,
1455 n=4 HFD) and *Adcy3ΔAT* (n=9 chow, n=4 HFD) mice. (**e-g**) Quantification of mean (**e**) nocturnal
1456 locomotor activity (LMA, **f**) daily respiratory exchange ratios (RER) and (**g**) daily oxygen
1457 consumption in chow-diet fed, male *LoxP* (n=7) and *Adcy3ΔAT* (n=9) mice. Bar graphs represent
1458 mean ± SD with all data points plotted. Unpaired, two-tailed Student's t-tests were performed to
1459 assess statistical significance. *P*-values are indicated within the panel. (**i-j**) Oxygen consumption
1460 rates (**i**) and extracellular acidification rates (**j**) in 1°iWA derived from SVF of *LoxP* or *Adcy3ΔAT*
1461 mice after injection with 10 µM CL316243. The numbers of measured wells are indicated in the
1462 panel and reflect BA from 2-3 independent mice. (**k-l**) Oxygen consumption rates (**k**) and
1463 extracellular acidification rates (**l**) in 1°iWA derived from SVF of *LoxP* or *Adcy3ΔAT* mice. OM,
1464 oligomycin; FCCP, AA/Rot, Antimycin A plus Rotenone. The numbers of measured wells are
1465 indicated in the panel and reflect BA from 2-3 independent mice. (**m-o**) Bar graphs represent mean
1466 ± SD with all data points plotted. Statistical significance was determined by performing Two-Way
1467 ANOVA with repeated measurements for x values (mixed models). *Post-hoc P*-value correction to
1468 account for multiple testing was performed using Bonferroni adjustment. The source of variation,
1469 % of the variation and exact *P* values are given in the table insets. (**d,h-l**) Bar graphs represent
1470 mean ± SD with all data points plotted. Statistical significance was determined by performing Two-
1471 Way ANOVA with repeated measurements for x values (mixed models). *Post-hoc P*-value
1472 correction to account for multiple testing was performed using Bonferroni adjustment. The source
1473 of variation, % of the variation and exact *P* values are given in table insets.
1474
1475 **Supplementary Figure S6: ADCY3-AT alters ADCY3 subcellular localization and limits**
1476 **cAMP biosynthesis.** (**a-b**) Analysis of STK activity in *Adcy3ΔAT* BAT. Kinome trees depict the
1477 mean kinase statistic of differentially activated STKs in (**a**) *Adcy3ΔAT* vs. *LoxP* (22°C) and (**b**)
1478 *Adcy3ΔAT* (22°C) vs. *Adcy3ΔAT* (5°C, 6 days). (**c-d**) Comparison of *Adcy3ΔAT* vs *LoxP* at 22°C
1479 (**c**) and *Adcy3ΔAT* vs *LoxP* after 6 days at 5°C (**d**). At 22°C, a set of kinases is inversely regulated
1480 in BAT of *Adcy3ΔAT* and *Adcy3AdcKO* mice compared to *LoxP* mice. The mean kinase statistic of
1481 these kinases is shown for 22°C (**c**) and for 5°C (**d**). Data includes n = 4 biological replicates for
1482 all conditions. (**e**) Quantification of the average HA-signal intensity within the PM (co-localization
1483 with mCherry) and the ER (co-localization with calnexin). Data shown as mean + SD (empty
1484 vector: n=4; ADCY3-AT: n=8, ADCY3-FL: n=10). (**f**) Ratio PM/ER distribution (empty vector:
1485 n=4; ADCY3-AT: n=8, ADCY3-FL: n=10). Bar graphs represent mean ± SD with all data points
1486 plotted. An unpaired, two-tailed, and non-parametric Mann-Whitney tests were performed to assess

1487 statistical significance. If relevant, *P*-values are indicated within the panel. (**g**) Quantification of
1488 extracellular biotinylation of ADCY3-FL when co-expressed with mCherry or ADCY3-AT
1489 (mCherry: n=4, ADCY3-AT: n=4). (**h**) Quantification of intracellular cAMP levels using ELISA.
1490 CHO cells stably expressing ADCY3-AT or ADCY3-FL, or empty vector transfected CHO cells
1491 were stimulated with DMSO or 2 µM Forskolin for 30 min. Values were normalized to DMSO
1492 control and normalized to the respective amount of total protein (empty vector: n=4; ADCY3-AT:
1493 n=5, ADCY3-FL: n=5) (**i**) Quantification of intracellular cAMP levels using ELISA. CHO cells
1494 stably expressing ADCY3-AT or ADCY3-FL, or empty vector transfected CHO cells were
1495 stimulated with buffer or 1 µM Isoproterenol for 15 min. Values were normalized to the respective
1496 buffer control and normalized to the respective amount of total protein (empty vector: n=4;
1497 ADCY3-AT: n=5, ADCY3-FL: n=5) (**e-i**) Data is shown as mean ± SD with all data points plotted.
1498 To test for statistical significance, non-parametric (ranked) Kruskal–Wallis one-way analysis of
1499 variance (ANOVA) tests with Dunn's correction for multiple testing were performed. *P*-values are
1500 indicated in the panel.
1501
1502 **Supplementary Figure S7: Conserved and cold-inducible PPARGC1A-AT drives *Adcy3-at***
1503 **expression in BAT.** (**a**) Mammalian phylogeny from Meredith et al [77] modified in iTOL[89], with
1504 silhouettes in black indicating representative species that were selected for comparative analyses
1505 of PPARGC1A-AT. (**b**) Genomic conservation among representative rodents of *Adcy3-at* identified
1506 in the mouse. Color gradient indicates percent nucleotide identity of the *Adcy3-at* relative to the
1507 mouse. Phylogeny based on Swanson et al [91]. (**c**) Genomic conservation among representative
1508 primates of *Adcy3-at* identified in the human. Color gradient indicates percent nucleotide identity
1509 of *Adcy3-at* relative to the human. Phylogeny based on Perelman et al [90]. (**d**) Nucleotide sequence
1510 alignment of *Ppargc1a-at* (exon 1b) from various mammalian species. (**e**) Percent identity matrix
1511 of *Ppargc1a-at* among 14 representative mammals (exon 1b).
1512
1513 ***Supplementary tables:***
1514 Supplementary Table S1: Adipose depot-specific RNA-seq from cold-exposed C57BL/6 mice.
1515 Supplementary Table S2: Gene accession numbers for species conservation analyses.
1516 Supplementary Table S3: List of sgRNAs and primers for the generation of *Adcy3*ΔAT mice.
1517 Supplementary Table S4: List of SYBR qPCR primers
1518 Supplementary Table S5: List of locked nucleic acid (LNA) GapmeR inhibitors.

Figure 1: Transcriptional regulation of cAMP biosynthesis during cold adaptation of brown adipose tissue

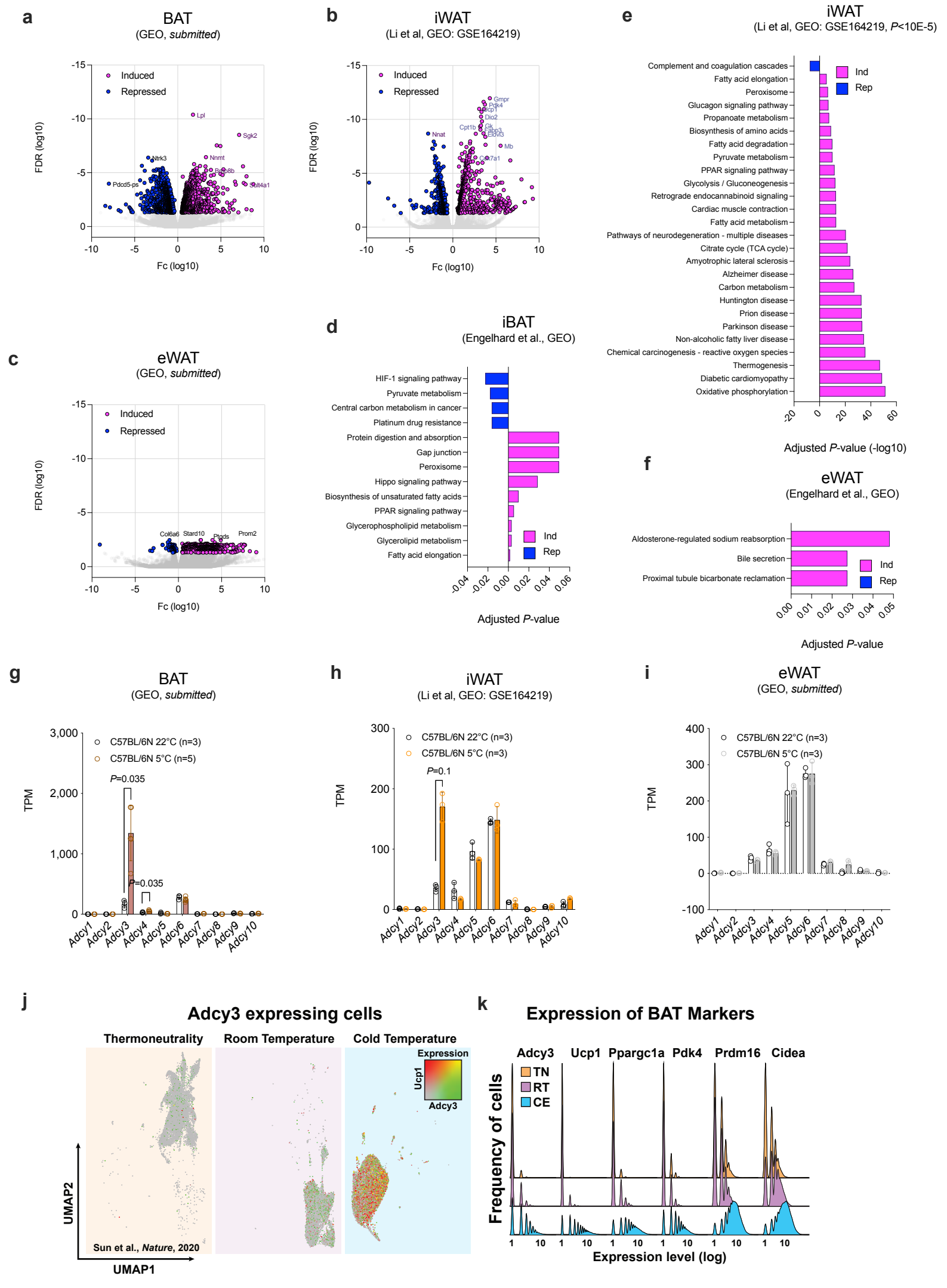

Figure 2: ADCY3 is required for cAMP biosynthesis in BAT and required for cold adaptation in obesity.

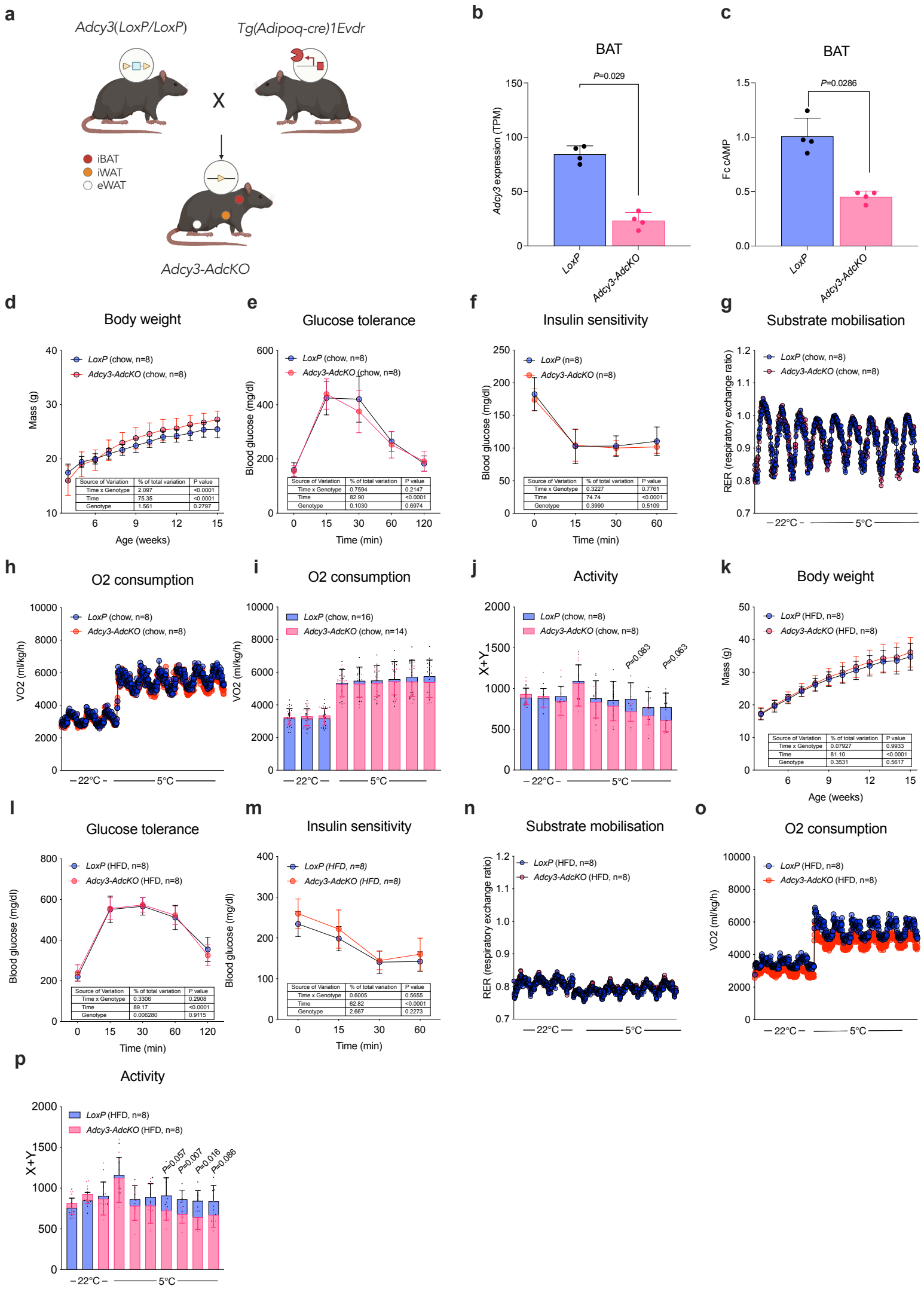

Figure 3: Active thermogenic adipocytes express a truncated ADCY3 (ADCY3-AT) transcript and protein isoform

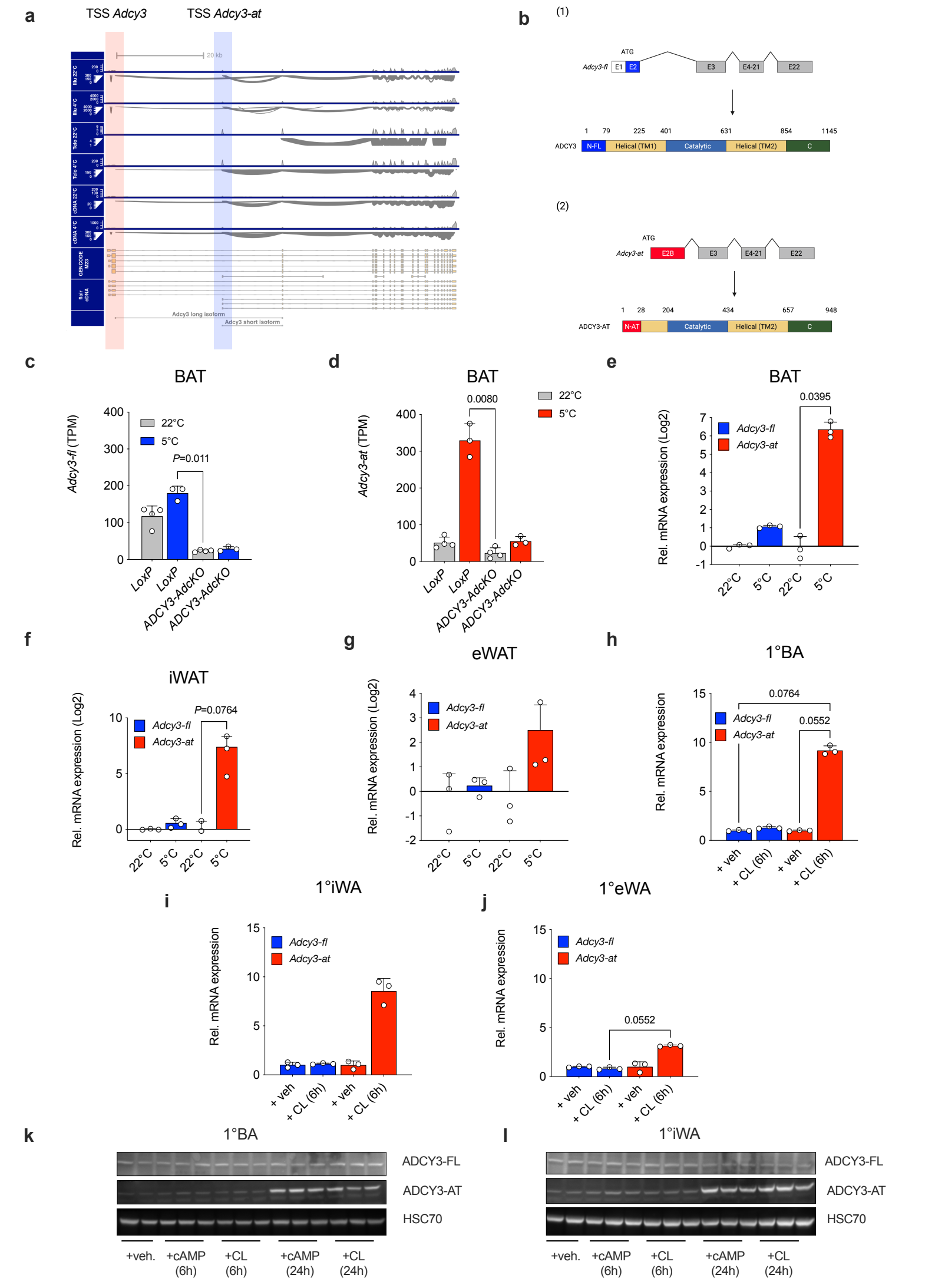

Figure 4: ADCY3-AT inhibits oxidative metabolism in vitro and in vivo

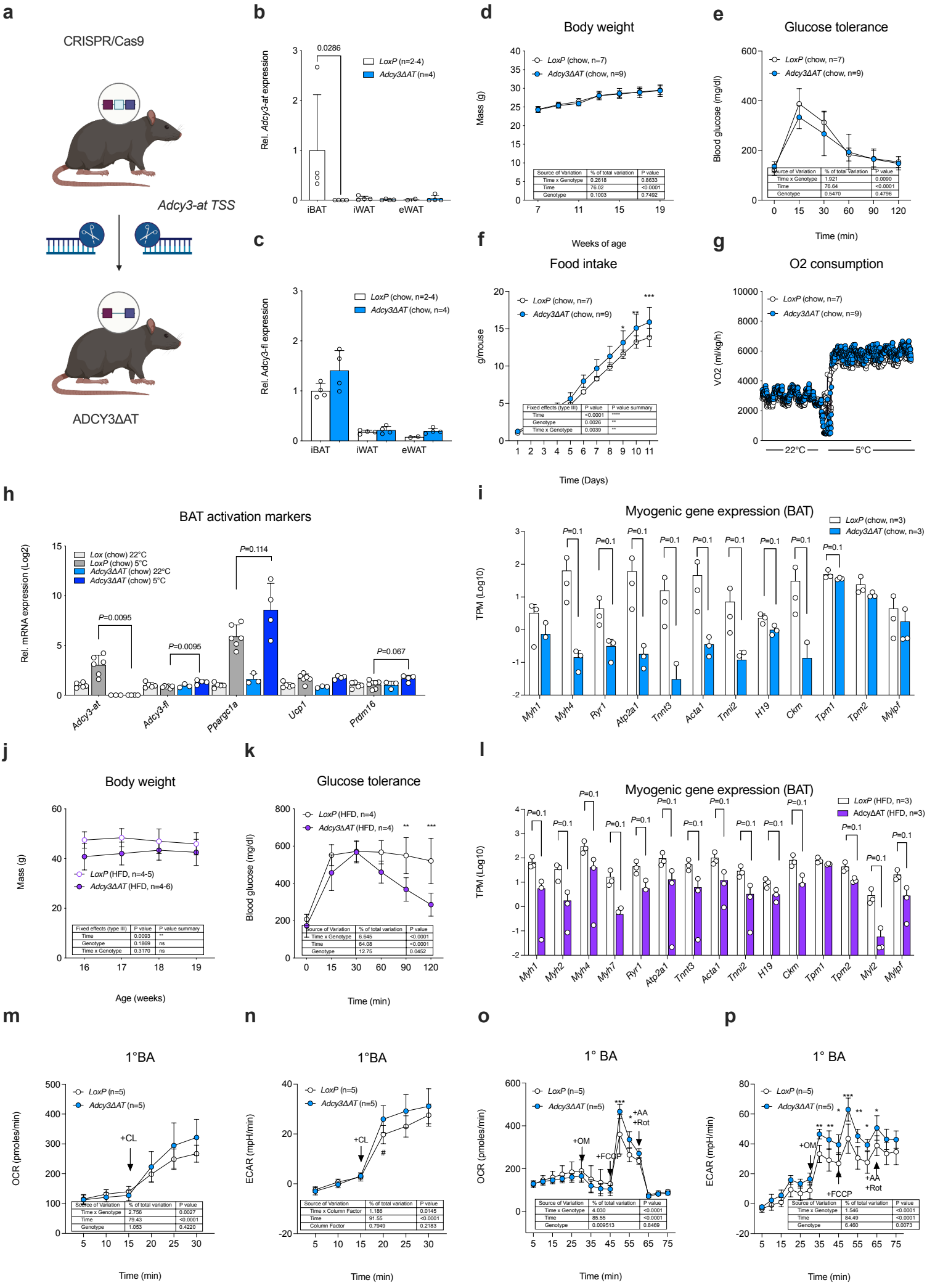

Figure 5: ADCY3-AT alters ADCY3-FL subcellular localisation and thereby limits cAMP biosynthesis

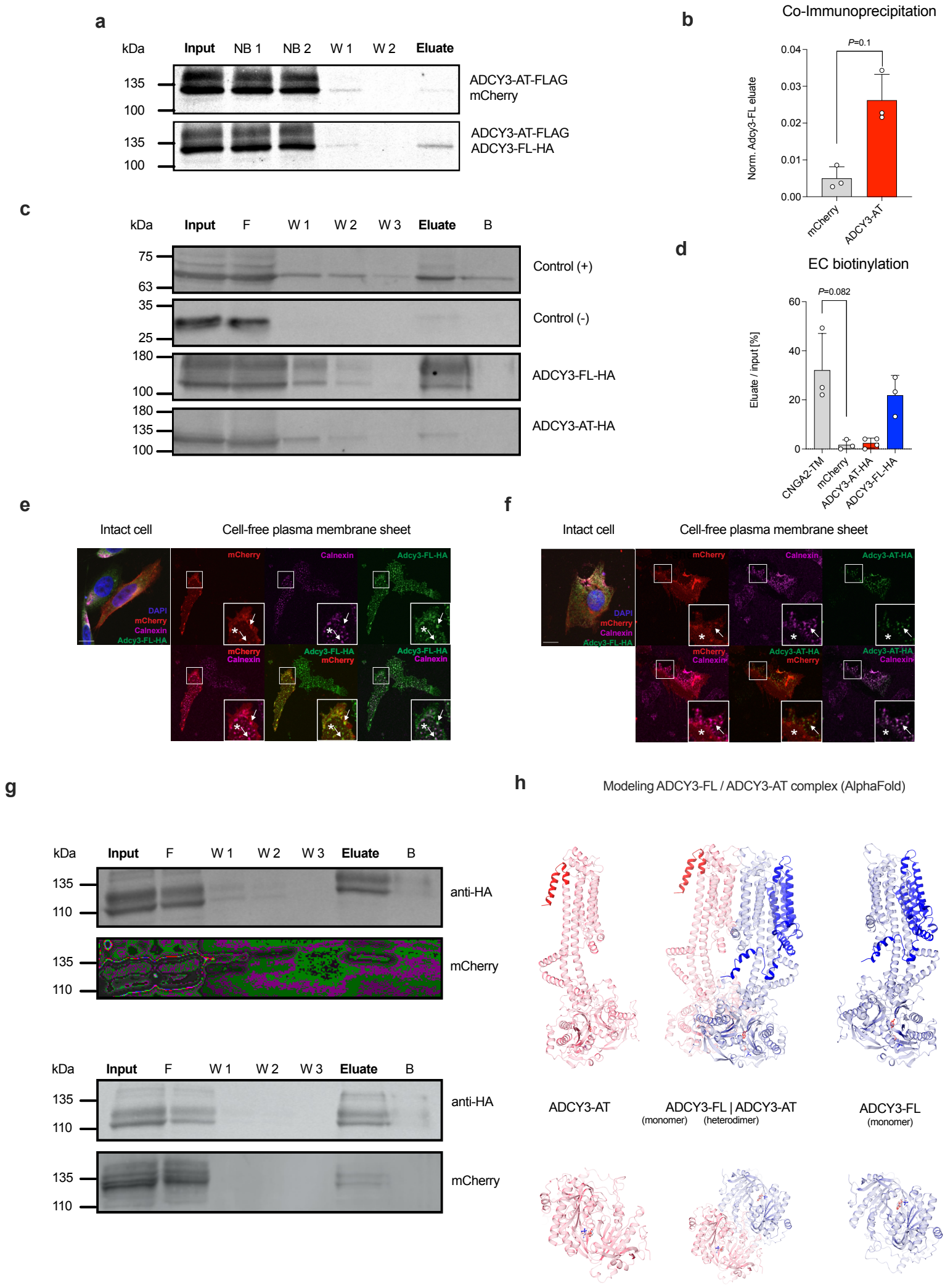

Figure 6: Conserved and cold-inducible PPARGC1A-AT drives *Adcy3-at* expression in brown adipocytes.

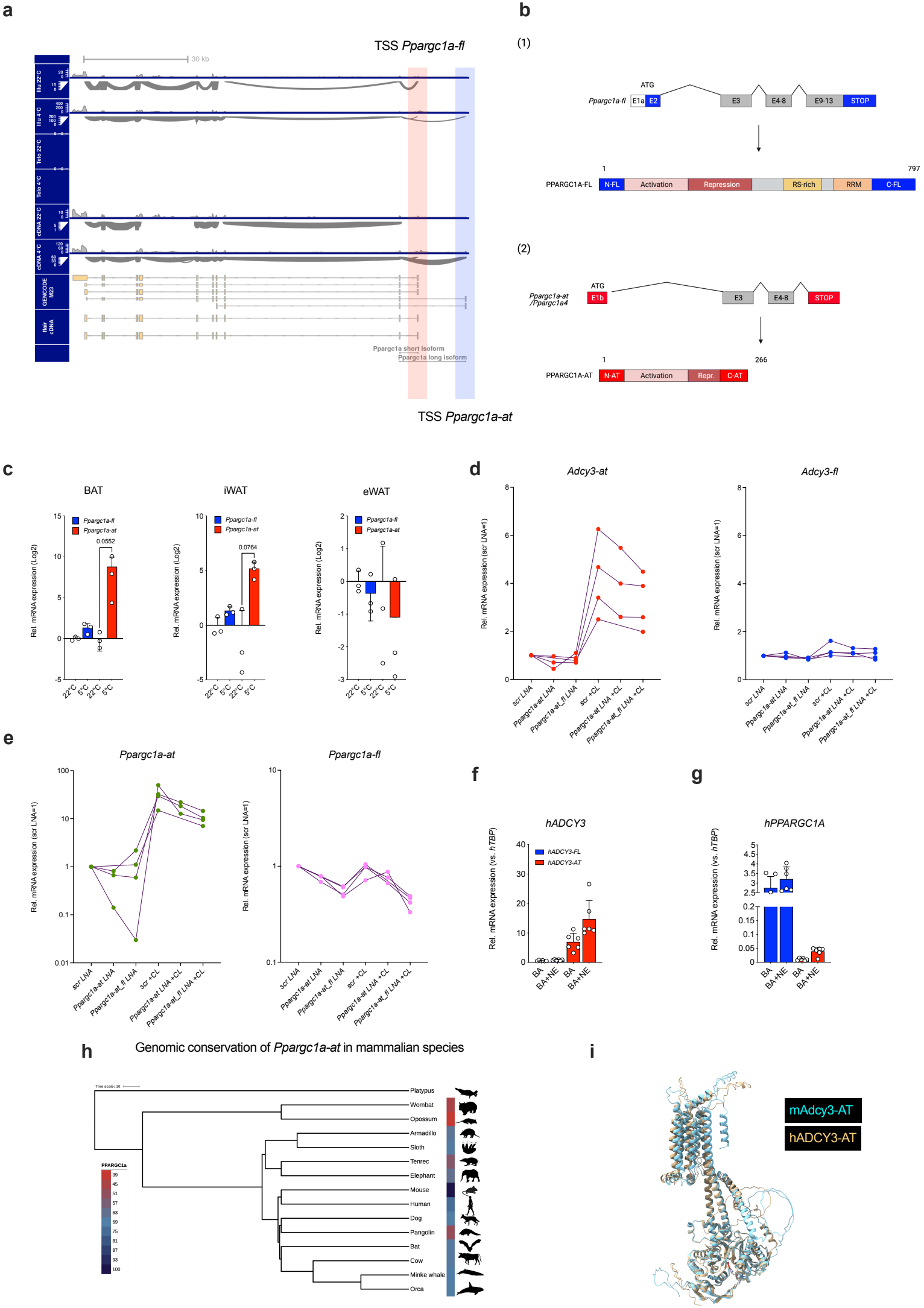

Figure S1: Transcriptional regulation of cAMP biosynthesis during cold adaptation of adipose tissue

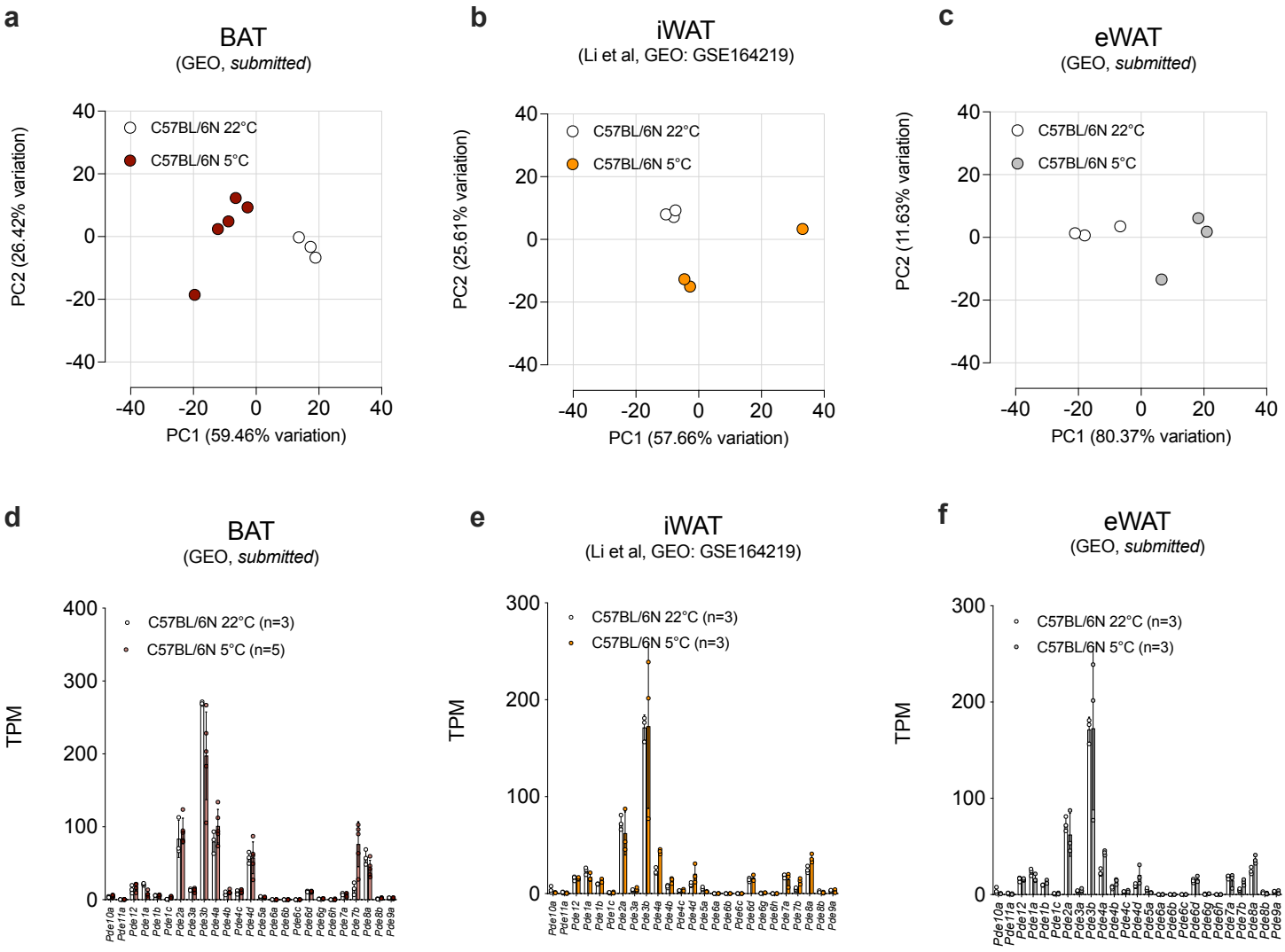

Figure S2: ADCY3 is required for cAMP biosynthesis in BAT and required for cold adaptation in obesity.

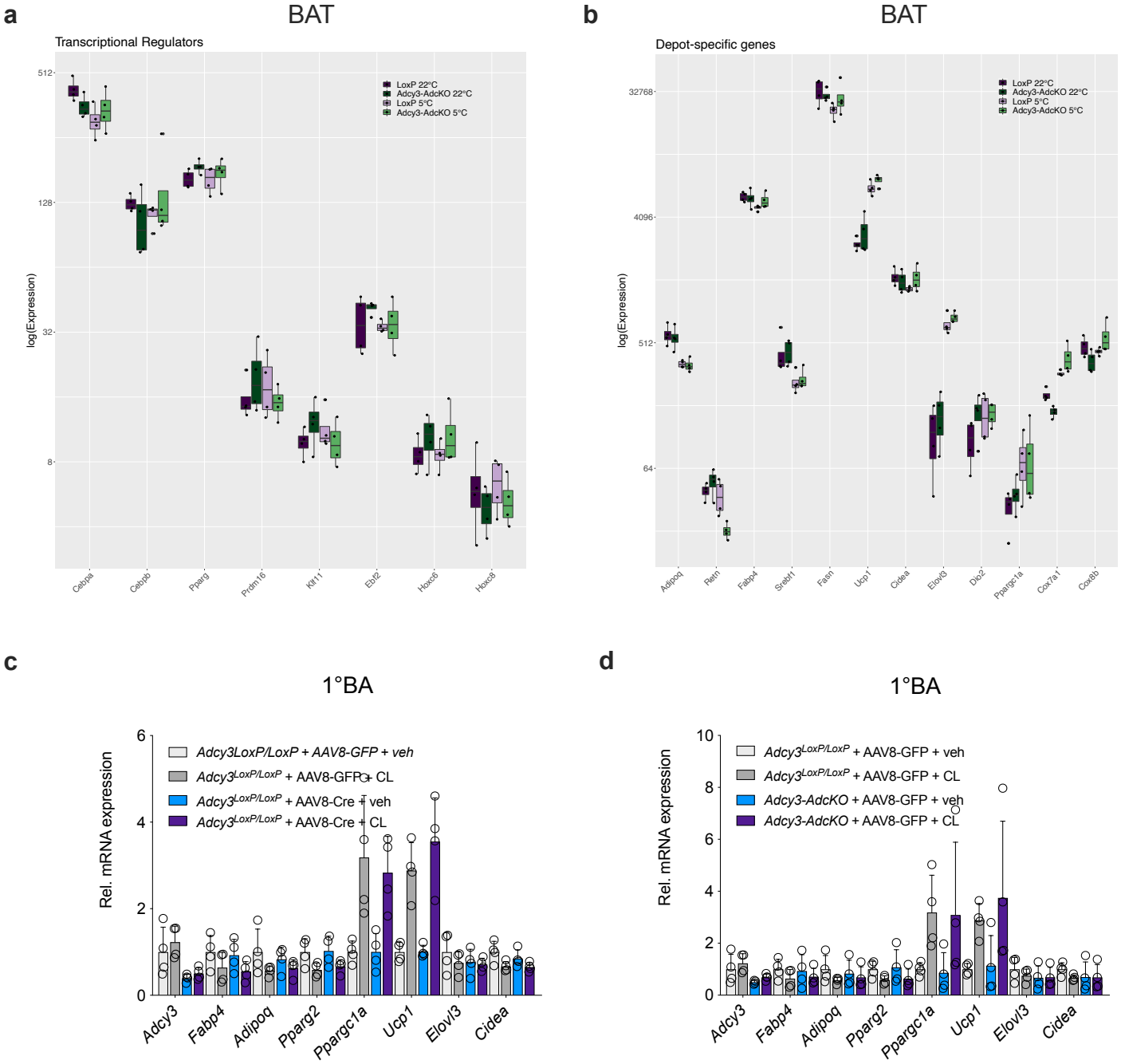

Figure S3: ADCY3 loss in adipocytes predisposes to obesity-associated brown fat dysfunction

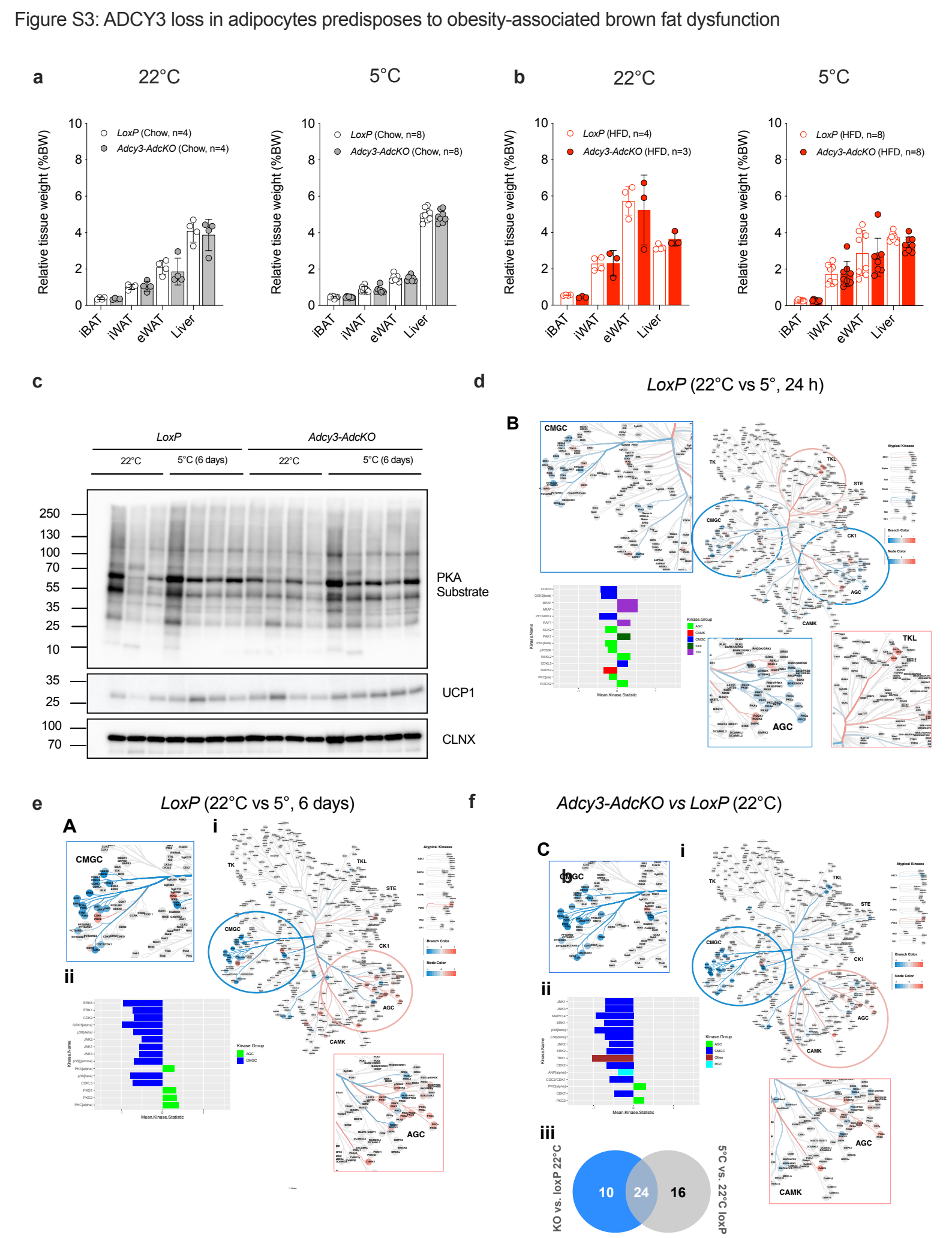

Figure S4: Active thermogenic adipocytes express a truncated ADCY3 (ADCY3-AT) transcript and protein isoform

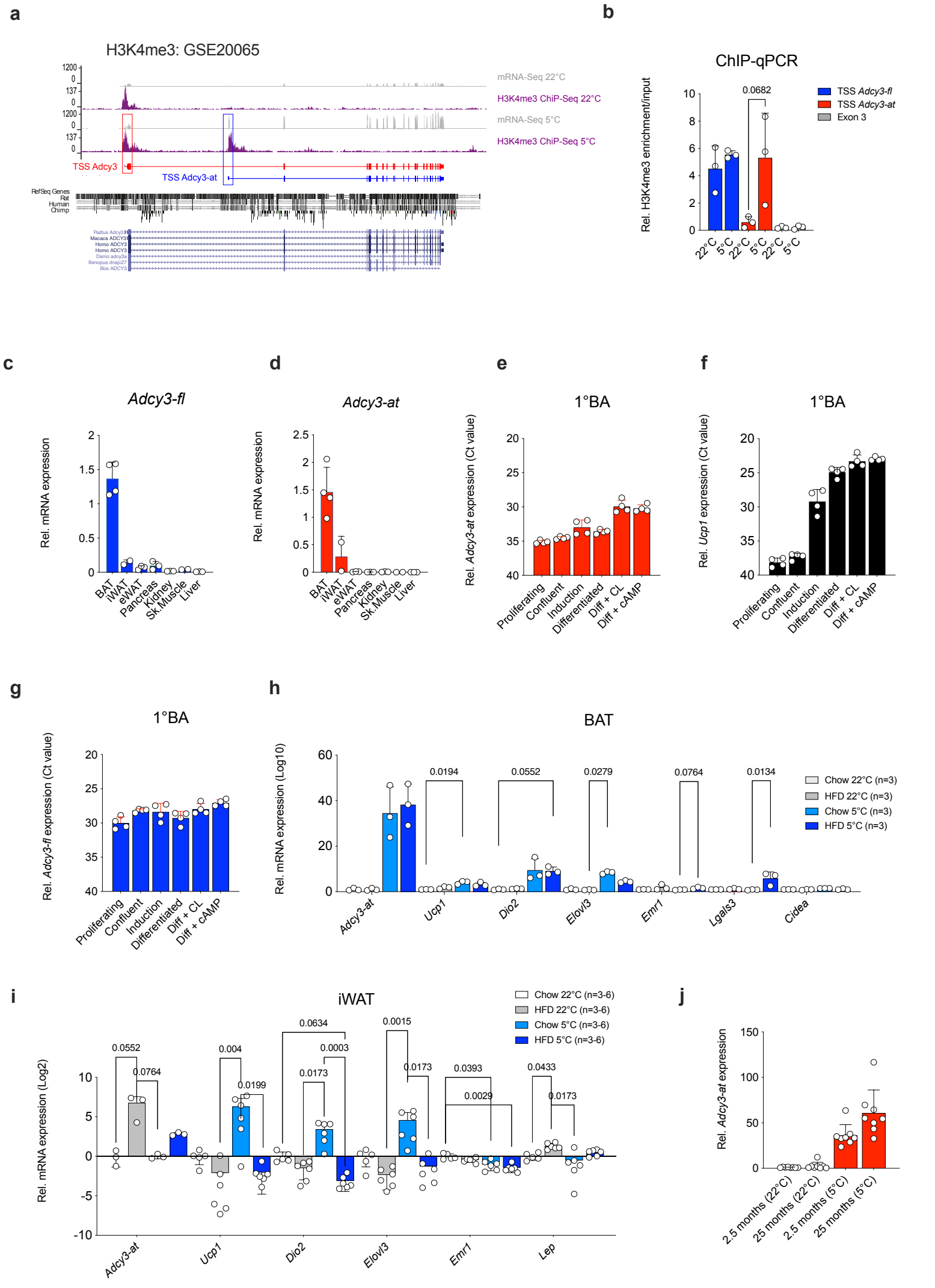

Figure S5: ADCY3-AT inhibits oxidative metabolism in vitro and in vivo

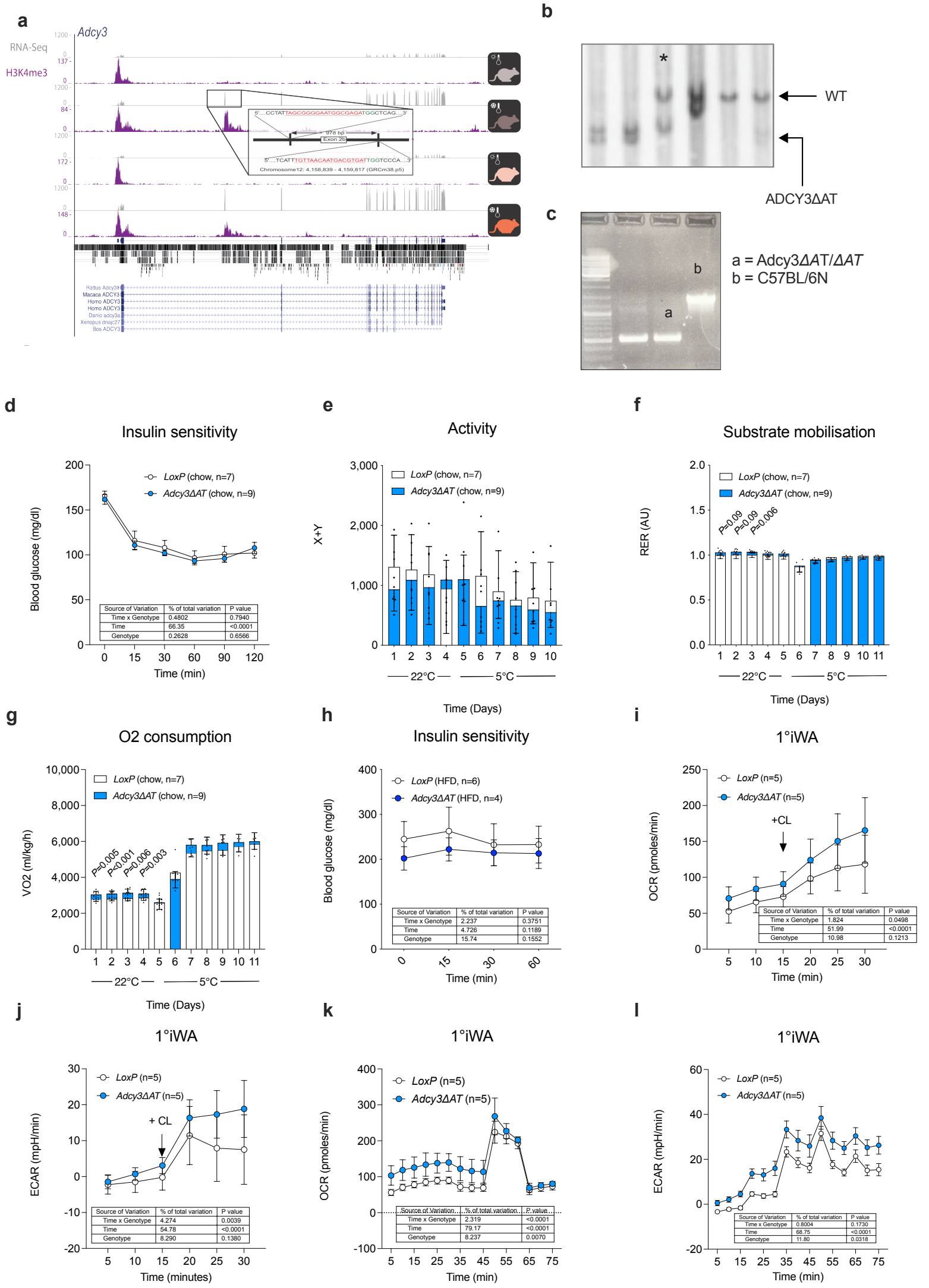

Figure S6: ADCY3-AT alters ADCY3-FL subcellular localisation and limits cAMP biosynthesis

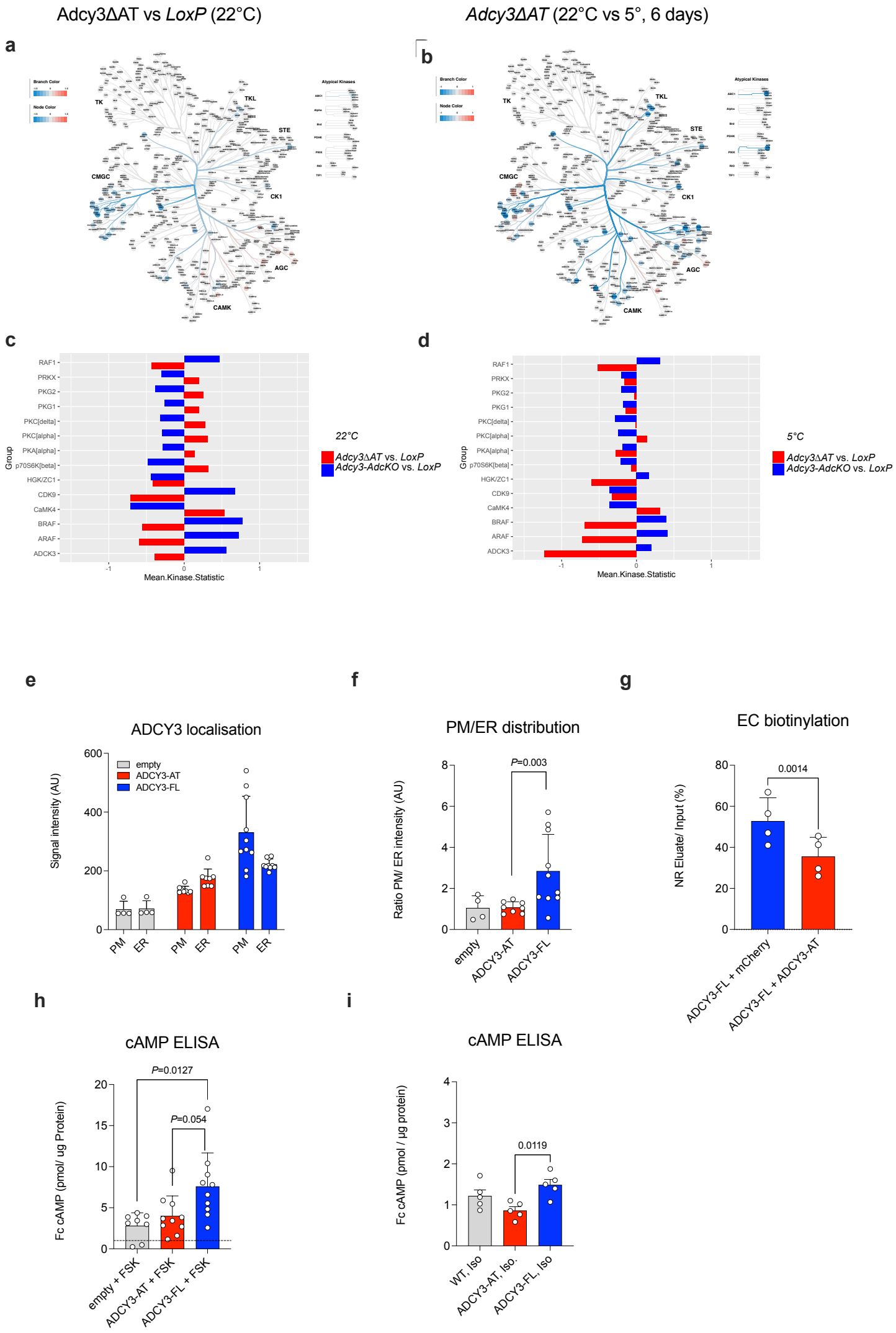

Figure S7: Conserved and cold-inducible PPARGC1A-AT drives *Adcy3-at* expression in BAT

a

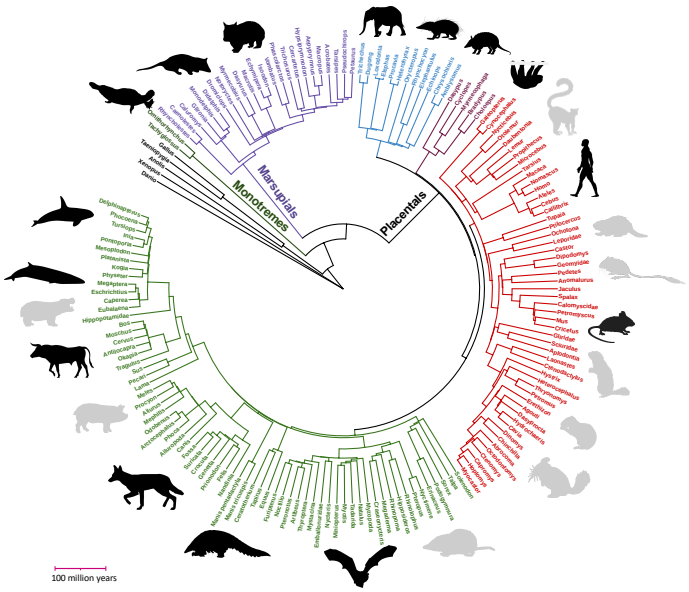

b Genomic conservation of *Adcy3-at* in rodent species

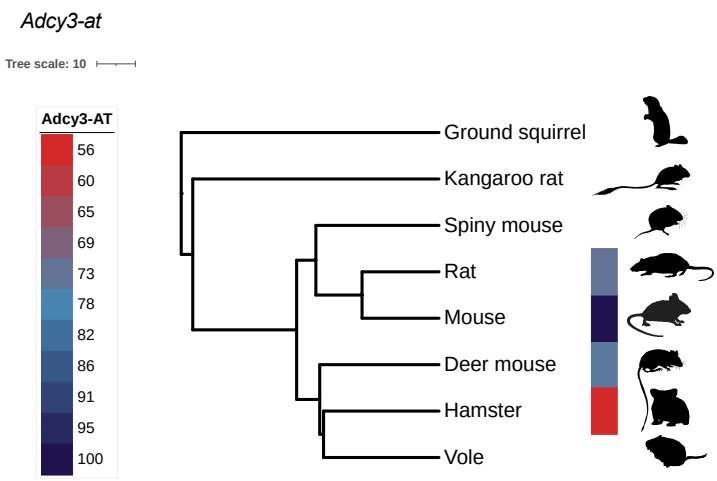

c Genomic conservation of *ADCY3- at* in primate species

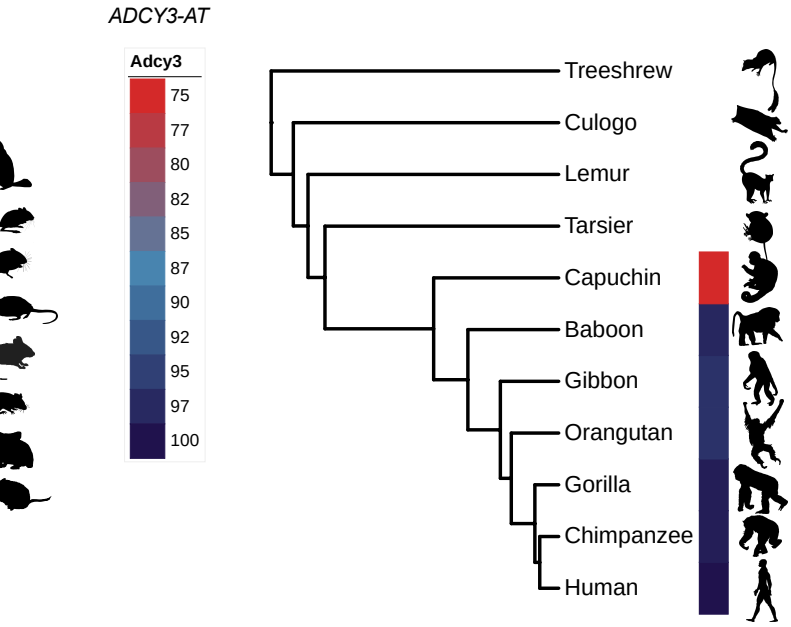

d Pairwise species comparision of *PPARGC1A-AT* genomic (exon 1b) sequence

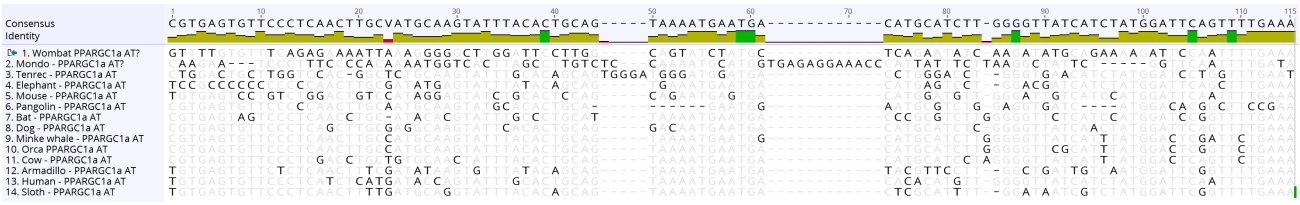

e Pairwise species comparision of *PPARGC1A-AT* genomic (exon 1b) sequence

	Wombat P...	Mondo – P...	Tenrec – P...	Elephant –...	Mouse – P...	Pangolin –...	Bat – PPA...	Dog – PPA...	Minke wha...	Orca PPAR...	Cow – PPA...	Armadillo ...	Human – ...	Sloth – PP...
Wombat PPARGC1a AT?		30.357%	33.333%	35.052%	45.361%	34.021%	37.755%	43.299%	40.816%	40.816%	38.776%	40.206%	41.237%	46.392%
Mondo – PPARGC1a AT?	30.357%		29.565%	41.071%	39.286%	30.000%	41.071%	40.179%	42.857%	39.286%	42.857%	38.393%	43.750%	38.393%
Tenrec – PPARGC1a AT	33.333%	29.565%		61.386%	54.902%	49.020%	61.165%	59.804%	60.194%	61.165%	63.107%	56.436%	56.863%	59.406%
Elephant – PPARGC1a...	35.052%	41.071%	61.386%		63.918%	55.670%	64.286%	68.041%	67.347%	67.347%	67.347%	71.875%	68.041%	70.833%
Mouse – PPARGC1a AT	45.361%	39.286%	54.902%	63.918%		50.515%	67.347%	69.072%	70.408%	69.388%	67.347%	65.979%	75.258%	68.041%
Pangolin – PPARGC1a ...	34.021%	30.000%	49.020%	55.670%	50.515%		62.245%	70.103%	71.429%	69.388%	65.306%	58.763%	58.763%	61.856%
Bat – PPARGC1a AT	37.755%	41.071%	61.165%	64.286%	67.347%	62.245%		75.510%	79.592%	81.633%	76.531%	70.408%	76.531%	75.510%
Dog – PPARGC1a AT	43.299%	40.179%	59.804%	68.041%	69.072%	70.103%	75.510%		84.694%	84.694%	82.653%	72.165%	81.443%	79.381%
Minke whale – PPARG...	40.816%	42.857%	60.194%	67.347%	70.408%	71.429%	79.592%	84.694%		95.918%	89.796%	73.469%	81.633%	80.612%
Orca PPARGC1a AT	40.816%	39.286%	61.165%	67.347%	69.388%	69.388%	81.633%	84.694%	95.918%		89.796%	73.469%	79.592%	80.612%
Cow – PPARGC1a AT	38.776%	42.857%	63.107%	67.347%	67.347%	65.306%	76.531%	82.653%	89.796%	89.796%		69.388%	77.551%	76.531%
Armadillo – PPARGC1...	40.206%	38.393%	56.436%	71.875%	65.979%	58.763%	70.408%	72.165%	73.469%	73.469%	69.388%		74.227%	82.292%
Human – PPARGC1a AT	41.237%	43.750%	56.863%	68.041%	75.258%	58.763%	76.531%	81.443%	81.633%	79.592%	77.551%	74.227%		82.474%
Sloth – PPARGC1a AT	46.392%	38.393%	59.406%	70.833%	68.041%	61.856%	75.510%	79.381%	80.612%	80.612%	76.531%	82.292%	82.474%	